Redox Biology 73 (2024) 103195

Contents lists available at ScienceDirect

Redox Biology

journal homepage: www.elsevier.com/locate/redox

Iron accumulation in ovarian microenvironment damages the local redox balance and oocyte quality in aging mice☆

Ye Chen [a], Jiaqi Zhang [b], Ying Tian [b], Xiangning Xu [b], Bicheng Wang [b], Ziqi Huang [b], Shuo Lou [b], Jingyi Kang [b], Ningning Zhang [b], Jing Weng [b], Yuanjing Liang [b], Wei Ma [b,*]

[a] Department of Pathology, Beijing Friendship Hospital, Capital Medical University, Beijing, 100050, China
[b] Department of Histology and Embryology, School of Basic Medical Sciences, Capital Medical University, Beijing, 100069, China

A B S T R A C T

Accumulating oxidative damage is a primary driver of ovarian reserve decline along with aging. However, the mechanism behind the imbalance in reactive oxygen species (ROS) is not yet fully understood. Here we investigated changes in iron metabolism and its relationship with ROS disorder in aging ovaries of mice. We found increased iron content in aging ovaries and oocytes, along with abnormal expression of iron metabolic proteins, including heme oxygenase 1 (HO-1), ferritin heavy chain (FTH), ferritin light chain (FTL), mitochondrial ferritin (FTMT), divalent metal transporter 1 (DMT1), ferroportin1(FPN1), iron regulatory proteins (IRP1 and IRP2) and transferrin receptor 1 (TFR1). Notably, aging oocytes exhibited enhanced ferritinophagy and mitophagy, and consistently, there was an increase in cytosolic Fe2+, elevated lipid peroxidation, mitochondrial dysfunction, and augmented lysosome activity. Additionally, the ovarian expression of p53, p21, p16 and microtubule-associated protein tau (Tau) were also found to be upregulated. These alterations could be phenocopied with in vitro Fe2+ administration in oocytes from 2-month-old mice but were alleviated by deferoxamine (DFO). In vivo application of DFO improved ovarian iron metabolism and redox status in 12-month-old mice, and corrected the alterations in cytosolic Fe^{2+}, ferritinophagy and mitophagy, as well as related degenerative changes in oocytes. Thereby in the whole, DFO delayed the decline in ovarian reserve and significantly increased the number of superovulated oocytes with reduced fragmentation and aneuploidy. Together, our findings suggest that aging-related disturbance in ovarian iron homeostasis contributes to excessive ROS production and that iron chelation may improve ovarian redox status, and efficiently delay the decline in ovarian reserve and oocyte quality in aging mice. These data propose a novel intervention strategy for preserving the ovarian reserve function in elderly women.

1. Introduction

The ovary is one of the organs that exhibit early-onset aging-associated dysfunction in human [1]. Ovary aging is characterized by decreases in follicle number and oocyte quality, primarily due to the gradual deterioration of the redox stress status in the ovarian microenvironment [2]. The immediate oocyte microenvironment consists of the surrounding cells, the extracellular matrix, and signaling molecules, including hormones, growth factors, and metabolic products [3]. The effects and molecular mechanisms of microenvironmental changes on oocyte quality during ovarian aging remain unclear and deserve more in-depth study.

Oxygen free radicals are a high-activity pro-oxidation group of molecules produced during aerobic metabolism, including reactive oxygen species (ROS) and reactive nitrogen species (RNS). Under normal physiological conditions, ROS are indispensable for ovarian follicle development and ovulation, however, uncontrolled ROS production can provoke oxidative stress effects, and usually participate in the occurrence and development of certain diseases, including a series of reproductive diseases, such as endometriosis and polycystic ovary syndrome [4–6]. ROS is considered as a key mechanism of ovarian aging, and is highly associated with spindle instability, chromosomal abnormalities, telomere shortening, biomacromolecular damage and reduced developmental competence in aging oocytes [7,8]. Currently, there is a pressing need to understand the upstream source of ROS in the ovarian microenvironment and to develop therapeutic measures tackling ovarian aging.

Dysregulated iron homeostasis is a hallmark of human aging, and is associated with an increased risk of many age-related diseases, such as cancers, cardiovascular, cerebrovascular and neurodegenerative

☆ This study was supported by grants from National Natural Science Foundation of China (82071641 and 81671454) and Natural Science Foundation of Beijing, China (7242003 and 7222002).

* Corresponding author. Department of Histology and Embryology, School of Basic Medical Sciences, Capital Medical University, 10 XiTouTiao, Youanmen, Beijing 100069, China.
E-mail address: mawei1026@ccmu.edu.cn (W. Ma).

https://doi.org/10.1016/j.redox.2024.103195
Received 18 April 2024; Received in revised form 12 May 2024; Accepted 15 May 2024
Available online 17 May 2024

disorders, and in principle, all these physiological and pathological processes are closely related to oxidative stress-induced cellular damages [9,10]. It has been widely accepted that iron overload frequently brings about high levels of cellular free divalent iron (Fe^{2+}), which usually stimulates the Fenton reaction, producing highly oxidative radicals, mainly the hydroxyl radical (•OH). ROS overproduction heavily consumes the cellular antioxidant capacity, including the activity of glutathione peroxidase 4 (GPX4), and thus enhances the peroxidation of polyunsaturated fatty acid (PUFA) in cells, ultimately leading to ferroptosis, a non-apoptotic iron-dependent form of cell death [11,12].

Cells establish a delicate balance between iron availability and storage, which is accomplished through the orchestrated action of a network of proteins involved in iron transport, import, export, storage, and a host of additional iron homeostasis regulatory circulating and intracellular proteins [13]. Most ferric ions (Fe^{3+}) in the plasma are loaded on transferrin (TF), and the TF - Fe^{3+} complex is delivered into cells under the facilitate of transferrin receptor 1 (TFR1). After the iron is dissociated, TFR1 is recycled to the surface of the cell membrane, and ferric ions are reduced back to ferrous ions (Fe^{2+}), which are transported and released via metal-ion transporter 1 (DMT1) in the proton coupling model [14]. Free iron is either utilized in metabolic processes, such as the synthesis of hemoglobin and Fe–S cluster or sequestered in the cytosolic ferritin, including ferritin heavy chain (FTH), ferritin light chain (FTL) and mitochondrial ferritin (FTMT), serving as a cellular iron store [15]. Excess iron can be exported from the cell via ferroportin 1 (FPN1) [16,17]. The expression/translation of iron-related genes mentioned above is post-transcriptionally regulated by iron regulatory proteins 1 and 2 (IRP1 and IRP2), which sense cellular iron concentration [14,18]. Ferritin level is also regulated by autophagic degradation, a process mediated by nuclear receptor coactivator 4 (NCOA4), and known as ferritinophagy [16]. In addition, heme oxygenase-1 (HO-1) catalyzes the first and rate-limiting enzymatic step of heme degradation, producing carbon monoxide, biliverdin, and free iron, thereby involving iron homeostasis maintenance [19]. All the above proteins interact synergistically to maintain a dynamic iron homeostasis in cells under physiological conditions. As reported, these proteins become disordered in expression and function during aging, and are associated with age-related neurodegenerative diseases and neurotoxic ferric iron deposits [20]. Iron chelators such as deferoxamine (DFO) can reduce the availability of iron by chelating non-transferrin bound iron (free iron), iron in transit between transferrin and ferritin (labile chelating iron pool), hemosiderin and ferritin. Such agents are proven to reduce cellular iron uptake and limit ROS production, exhibiting therapeutic value in diabetes, neurodegenerative and neurovascular diseases [21].

After puberty, the ovaries present periodic follicular development, ovulation and luteinization [22]. Essentially, it means repeated process of vascular establishment, rupture, and bleeding along female reproductive life [23]. Particularly, the corpus luteum is one of the most vascularized organs in the body, it undergoes extremely rapid cellular and vascular changes during luteal establishment and degeneration [24]. For this reason, the ovary itself is a hemin-rich microenvironment, thereby the follicles may live in an iron overload condition. However, to our knowledge, no study has examined the changing pattern of iron metabolism in aging ovaries, especially the local iron status, and protein changes related to iron storage, transportation and distribution at organ and cell levels. So far there lacks a complete description about the exact relationship of ovarian iron status with the local ROS accumulation and the decline in oocyte quality and quantity, not to mention any intervention strategy on iron metabolism to improve fertility in elderly women. Here we found the iron regulatory network becomes disordered and iron content is highly elevated in mouse aging ovaries, free Fe^{2+} level is increased by elevated ferrinophagy and is closely associated with oxidative stress and degenerative changes in oocytes, these degenerative trends can be greatly alleviated by the iron chelating agent. These data imply that excessive iron accumulation is surely associated with ovary aging, and iron-chelating may be a feasible intervention strategy.

2. Material and methods

2.1. Animals

The animal experiment protocols were approved by the Animal Care and Use Committee of Capital Medical University, and carried out following the Administration Regulations on Laboratory Animals of Beijing Municipality. The female Balb/c mice aged at 2 months and 6 months, and retired breeding mice at age of 8 months were obtained from Vital-River Experimental Animal Technology, Co, Ltd. (Beijing, China). Some retired breeding 8 months Balb/c mice were from our research group. All the aging mice were raised for 4 months before conducting experiments. All mice were housed and fed in a temperature-controlled room with a 12 h light-dark cycle and free access to food and water. For iron chelation with Deferoxamine (DFO) in vivo, 12-month-old mice were injected intraperitoneally with DFO (HY–B0988, MCE) at 100 mg/kg body weight at 16:00 o'clock every day for 14 consecutive days. Mice injected with the same volume of phosphate buffer saline (PBS) were used as control.

2.2. Estrous cycle detection

All females underwent estrous cycle monitoring between 9:00 and 10:00 o'clock in the morning, by analyses of vaginal smears. Briefly, 10 μl of saline was injected into the vagina and recollected by suction 3 times, then smeared on a slide, and dried in air. The smear was fixed with 95 % ethanol and processed for hematoxylin-eosin staining. All mice involved in ovarian level testing have undergone estrus cycle testing, and only the mice in the dioestrum were used for further analysis.

2.3. Hematoxylin-eosin (HE) staining and ovary follicle counting

HE was carried out to identify ovarian structure and developing follicles. Mice were perfused with 4 % paraformaldehyde, bilateral ovaries were extracted in normal saline and fixed in 4 % paraformaldehyde, then dehydrated and embedded in paraffin. Paraffin-embedded tissues were consecutively cut into slices with a thickness of 4 μm. The slices were dewaxed by dimethylbenzene after 1 h of heating at 60 °C, and immersed in absolute alcohol, 95 % alcohol, 85 % alcohol, and 75 % alcohol, respectively, for 5 min each. After being processed with the HE staining procedure, the slices were dehydrated by gradient alcohol and xylene, and finally mounted.

The follicle stages were classified according to Pederson's standard [25]. n brief, a primordial or primary follicle is composed with an oocyte surrounded by a single layer of flattened or cubical granulosa cells; a secondary follicle consists of an oocyte and more than one layer of cuboidal granulosa cells with no visible antrum; an antral follicle refers to a follicle possessing a clearly antral space containing follicular fluid. For the follicle count, each follicle was tracked consecutively, from the appearance of the follicle to the observation of the oocyte nucleus and then to the disappearance of the follicle, which was counted as a follicle.

2.4. Prussian blue staining and masson staining analysis and scoring

As described in the above steps, the dewaxed slices of ovarian tissue were processed for Prussian blue staining (G1424, Solarbio) and Masson staining (G1346, Solarbio), according the instructions introduced by the manufacturer. After dehydrated by gradient alcohol and xylene, the slices were mounted and analyzed with an automatic Slide Scanner. The percentage of Prussian blue and Masson positive areas was calculated by IHC Toolbox of Image J software (Image J).

2.5. Immunohistochemistry analysis and scoring

After repaired with sodium citrate at high temperature and pressure, the ovarian tissue slices were blocked with normal goat serum for 1 h and then incubated in primary antibodies to 4-HNE or 8-OHdG, specific antibody information is shown in the supplement, at 4 °C overnight. After washed with PBS 3 times, the slices were treated with horseradish peroxidase-conjugated secondary antibodies for 1 h at room temperature, and then followed by color-reaction with a DAB visualization kit (ZLI-9017, ZSGB), and nucleus labeling with hematoxylin. After that the slices were dehydrated, mounted and analyzed as mentioned above.

2.6. Oocyte collection and culture

Female mice were euthanatized with CO_2 at 44–48 h after intraperitoneal administration of 10 IU pregnant mare serum gonadotropin (PMSG, Ning Bo Second Hormone Factory). The ovaries were isolated and transferred into Hepes-buffered Minimum Essential Medium (HEPES-MEM), and cumulus-oocyte complexes (COCs) were released from the ovarian follicles punctured using 25-gauge needles. COCs were cultured in MEM with 3 mg/ml bovine serum albumin (BSA, Sigma) and 10 % fetal bovine serum (FBS, Gibco), in an incubator with 5 % CO_2 and saturated humidity at 37 °C. After cultured for 8 h, corresponding to the meiotic stage at metaphase I (MI), the surrounding cumulus cells were removed by gentle pipetting, and the denuded oocytes were collected for further analysis. To collect ovulated MII oocytes, 10 IU human chorionic gonadotrophin (hCG, Ning Bo Second Hormone Factory) was administered via intraperitoneal injection at 44–48 h after PMSG treatment. At 14 h after hCG injection, the mice were sacrificed with CO_2, and the oviducts were removed from each mouse. COCs were released in HEPES-MEM by puncturing the oviducts under a microscope. MII oocytes were derived from the surrounding cumulus cells by a short incubation in 0.1 % hyaluronidase (H3506, Sigma) and selected for counting and further use.

2.7. Treatment of ammonium iron (II) sulfate hexahydrate (FAS) and deferoxamine (DFO)

FAS (BCCC7977, Sigma-alorich) and DFO (HY–B0988, Medchemexpress) were dissolved in MEM. GV oocytes from 2-month-old mice were incubated with 3000 μM FAS or 3000 μM FAS +3000 μM DFO for 6 h, and then collected for live cell fluorescence detection. Similarly, GV oocytes from 12-month-old mice were treated with 3000 μM DFO in MEM for 6 h or 16 h, and then processed for analysis.

2.8. Inductively coupled plasma-mass spectrometry (ICP-MS)

In order to assay iron content in ovarian tissue of naturally aging mice, the ovaries were harvested from mice at the age of 2 months, 6 months, 12 months and 18 months, respectively. Tissues of liver and hippocampus were also collected in the same chronological order, and used as parallel controls. After thoroughly rinsed off the blood in PBS and suck dry with absorbent paper, the tissues were weighed and measured, and nitrated with nitric acid (3 ml) and hydrogen peroxide (1 ml) in a microwave accelerated reaction/digestion system (MARS5, CEM). The sample solution was titrated to 8–10 ml. Similar measurements were also carried out in tissues of the hippocampus and livers for use as parallel controls. Forty denuded oocytes were stored in 1 ml ultrapure water, and nitrated with nitric acid (1 ml) for 1 h at 80 °C. The oocyte sample solution was titrated to 5 ml. After building the curve of the fitting standard (GSB 04-1767-20041), the samples were injected into the ICP-MS instrument (8800, Agilent) for iron content determination.

2.9. Western blot (WB)

80-150 denuded oocytes in each sample were collected in Laemmli sample buffer (1610737, Bio-Rad) supplemented with protease inhibitor cocktail (P2714, Sigma), and boiled for 10 min. For ovarian tissue samples, the unilateral ovary of a mouse was placed in 50–80 μl RIPA Lysis Buffer (Beyotime Biotechnology) containing protease inhibitors and phosphatase inhibitors (Roche) and disrupted with a grinder (Tiangen). The BCA method was used to determine supernatant protein concentrations. Then the prepared protein solution was mixed with 5X loading buffer, and boiled for 10 min. The proteins were separated on 10 % SDS-PAGE and blotted to PVDF membranes (IPVH00010, Millipore) at a current of 250 mA for 1.5 h. The membranes were blocked in 5 % fat-free milk in Tris-buffered saline (TBS) containing 0.1 % Tween-20 (TBST) for 1 h at room temperature, and then incubated overnight at 4 °C in diluted primary antibodies. Specific antibody information is shown in the supplement table1. After washing three times with TBST for 20 min each, the membranes were treated in horseradish peroxidase-conjugated secondary antibodies for 1 h at room temperature. After thorough washing, the bands were visualized with an enhanced chemiluminescence system (E412-01, Vazyme) and imaged with Bio-Rad gel imager. The blots were processed for semiquantitative grayscale analysis using Image J software.

2.10. Detection of cellular catalytic Fe^{2+}, lysosome and mitochondria

Catalytic Fe^{2+}, lysosome and mitochondria were detected with a fluorescent turn-on probe, FeRhonox-1 (FerroFarRed, Goryo Chemical), LysoTracker Green (Beyotime Biotechnology) and MitoTracker Red (Beyotime Biotechnology), respectively, as previously described [26]. The denuded oocytes were incubated for 1 h at 37 °C in MEM with 20 μM FeRhonox-1, 2 μM LysoTracker Green, 600 nM MitoTracker Red and 20 nM Hoechst. After being washed, the oocytes were settled in fresh M2 medium and examined with a Confocal microscope (TCS SP8, Leica). The excitation/emission used for FeRhonox-1, LysoTracker, MitoTracker and Hoechst probes were 633/670, 504/511, 579/599 and 350/461 nm, respectively. Signal intensity was further analyzed with Image J Software.

2.11. Detection of cellular ROS

The denuded oocytes were labeled with 10 μM dichlorofluorescein diacetate (DCFH-DA) green, 600 nM MitoTracker Red (Beyotime Biotechnology) and 20 nM Hoechst in MEM for 30 min at 37 °C. After carefully washing and settling in fresh M2 medium, the oocytes were observed with a confocal microscope (TCS SP8, Leica). The excitation/emission used for ROS, MitoTracker and Hoechst probes were 504/511, 579/599 and 350/461 nm, respectively. The intensity of each fluorescence signal was analyzed with Image J Software.

2.12. Annexin-V staining

For the detection and quantification of apoptosis activity, the denuded oocytes were processed with the Annexin-V staining kit, according to the manufacturer's instruction (Beyotime Biotechnology). Briefly, the oocytes were incubated with 180 μl of binding buffer containing 20 μl of Annexin-V-FITC and 20 nM Hochest for 30 min at 37 °C. The oocytes were washed and settled in M2 medium, followed by observation and photograph with a confocal microscope (880, ZEISS). The excitation/emission used for Annexin-V and Hoechst probes were 504/511 and 350/461 nm, respectively. The signal intensity of Annexin-V was analyzed with Image J software.

2.13. Mitochondrial membrane potential

Mitochondrial membrane potential was assessed by JC-1 (HY-15534,

MCE), a fluorescent lipophilic carbocyanine dye. The denuded oocytes were co-stained with 400 nM JC-1 and 20 nM Hoechst in MEM for 30 min at 37 °C. After proper washing, the oocytes were placed in fresh M2 medium, then observed and photographed with a confocal microscope (880, ZEISS). JC-1 fluoresces green as a monomer and demonstrates potential-dependent accumulation in the mitochondria causing J-aggregate formation within polarized mitochondria and red fluorescence. A decrease in J-aggregates produces a red (≈590 nm) to green (≈529 nm) fluorescence emission shift and indicates mitochondrial depolarization. The signal intensity of the oocytes was analyzed with Image J software for the determination and comparison of red:green ratio.

2.14. Anti-müllerian hormone (AMH) enzyme-linked immunosorbent assay

The mouse blood collected from the heart was placed at room temperature for 2 h, then centrifuged at 3000 g for 20 min, the supernatant was harvested and processed for serum AMH measurement with an ELISA kit (E-EL-M3015, Elabscience Biotechnology), according to the manufacturer's protocol. The relative value was determined by Synergy H4 Hybrid Reader (BioTek).

2.15. Chromosomal spreading

MII oocytes without cumulus cells were gotten rid of zona pellucida by 2-min soak in acid Tyrode's solution (T1788, Sigma) at 37 °C [27]. After a short recovery in pre-warmed HEPES-MEM, the oocytes were transferred into 20 μl hypotonic fixative (1 % PFA with 0.1 % Triton X-100 in distilled water) on glass slides. The cells were dilated, ruptured, and finally disintegrated on slides. The slides were air-dried at room temperature and stored at −20 °C before use. Prior to 1 h blocking in 1 % BSA, slides were immersed in adequate PBS to wash off salts mixed in the chromosome samples [28,29]. The samples were immune-stained with human centromere auto serum (CREST) (1:100; 90C-CS1058, Fitzgerald) and counterstained with mounting medium containing DAPI, then analyzed with ZEISS microscopic system and Image J software as stated above.

2.16. Immunofluorescence

Denuded oocytes were fixed in 1 % paraformaldehyde (PFA) in PEM buffer (100 mM Pipes, 1 mM $MgCl_2$, and 1 mM EGTA, pH 6.9) with 0.5 % Triton X-100 for 1 h at room temperature. After washed in PBST (phosphate-buffered saline with 0.02 % Triton X-100) 3 times, the oocytes were blocked in PBS containing 10 % normal goat serum and 1 % BSA, then incubated in diluted mouse monoclonal anti-acetylated tubulin (1:5000; T7451, Sigma) at 4 °C, overnight. After thoroughly washed in PBST, the oocytes were labeled with anti-mouse Alexa-488 (1:500; Molecular Probes) in the dark for 60 min at room temperature, then washed and mounted on slides with anti-fade mounting medium containing DAPI (H-1200, Vector Laboratories). The samples were examined using a fluorescent ZEISS microscope, and images were analyzed by using Image J software.

2.17. Statistical analysis

The results are presented as the mean ± SEM of three replicates at least. Student's t-test was used to analyze the differences between two groups. Whereas, the One-way ANOVA tests followed by Tukey's multiple comparisons test or Kruskal-Wallis multiple comparisons test were used for the comparisons between multiple groups. $P < 0.05$ was considered statistically significant, in each of the statistical tests. The statistical data were obtained using the Prism software package (version 6.0).

3. Results

3.1. Increasing iron content in aging mouse ovaries and oocytes

Histochemical staining and follicle counting demonstrated that the number of follicles at all levels decreases in ovaries with the female mice aging (Fig. 1A and B). The absolute content of iron in ovaries continuously increased along with mouse age, and the value was substantially higher in mice aged at 12 months and 18 months than at 2 months and 6 months, with the peak level at 18 months (Fig. 1C). Similarly, an increasing trend of iron content was also detected in hippocampus and livers with mouse aging, and statistically higher at 12 months and 18 months in hippocampus, and at 12 months in liver sample. When comparing 12-month-old samples with 2-month-old ones, the increase of iron content was obviously higher in ovaries (71.1 %) than hippocampus (31.6 %) and liver (47.2 %), with more significant difference between the ovaries and hippocampus. As showed in Fig. 1D, iron level in oocytes was greater elevated in mice aged at 12 months than 2 months. Together, these data clearly indicate there is increasing iron accumulation in ovaries and oocytes during mouse natural aging.

3.2. Disturbed iron metabolism regulation and elevated aging indexes in ovaries

Western blot procedure was conducted to assess any possible changes in the regulating system of iron homeostasis, including iron uptake, output, intracellular transportation and storage. As showed in Fig. 2, the protein levels of FTH, FTL and FTMT, responsible for iron storage, were substantially higher in the ovaries of mice aged at 12 months than at 2 months (Fig. 2 A line 1–3, D- F). In the same way, the levels of DMT1, which is in charge of intracellular iron transport, and FPN1, the cellular iron exporter, showed an increasing trend with age (Fig. 2 A line 4–5, G- H). TFR1, which is responsible for iron uptake from serum, was significantly reduced at 6 months and 12 months (Fig. 2 A line 6, I). The expression of heme oxygenase-1 (HO-1), which breaks heme down into ferrous iron, carbon monoxide and biliverdin [30], was apparently upregulated at 6 months and 12 months when compared with that at 2 months (Fig. 2 B line 1, J). In addition, the levels of IRP2 were prominently reduced from 6 months to 12 months, IRP1 seems to be following a similar trend (Fig. 2 B line 2–3, K- L). The protein level of NCOA4, which seizes ferritin protein from binding to Fe^{2+}, was enhanced outstandingly as early as 6 months, and remained high up to 12 months (Fig. 2 B line 4, M). Along with iron rise, there exhibited a growing tendency in the protein expression of p53, p21, p16 and Tau (Fig. 2C line 1–4, N-Q), which are typical markers of senescence and cellular degeneration, and associated with dysfunctional iron metabolism [31,32]. Unexpectedly, no significant changes were detected in GPX4 expression in the ovaries of mice at different ages (Fig. 2C line 5, R).

3.3. Oocyte quality decline with age is associated with iron homeostasis disturbance

For further analysis about iron metabolic changes in oocytes, Western blot was employed in oocytes from mice aged at 2 months and 12 months. As showed in Fig. 3, the critical iron storing protein FTH was substantially decreased in oocytes at 12 months (Fig. 3 A line 1, E), completely different from its increasing trend in the whole ovary tissue, but at the same time, FTL and FTMT were markedly increased (Fig. 3 A line 2–3, F- G). Apparently, DMT1 and FPN1 were also upregulated while TFR1 was downregulated in aging oocytes (Fig. 3 B line 1–3, H- J), this pattern is similar with that in ovaries. Unlike the simultaneous downregulation of IRP1 and IRP2 in aging ovaries, only IRP2 was significantly decreased but IRP1 was pronouncedly increased in aging oocytes (Fig. 3 B line 4–5, K- L). Moreover, NCOA4 and autophagic protein LC3-II were dramatically elevated while Beclin1 and SQSTM1

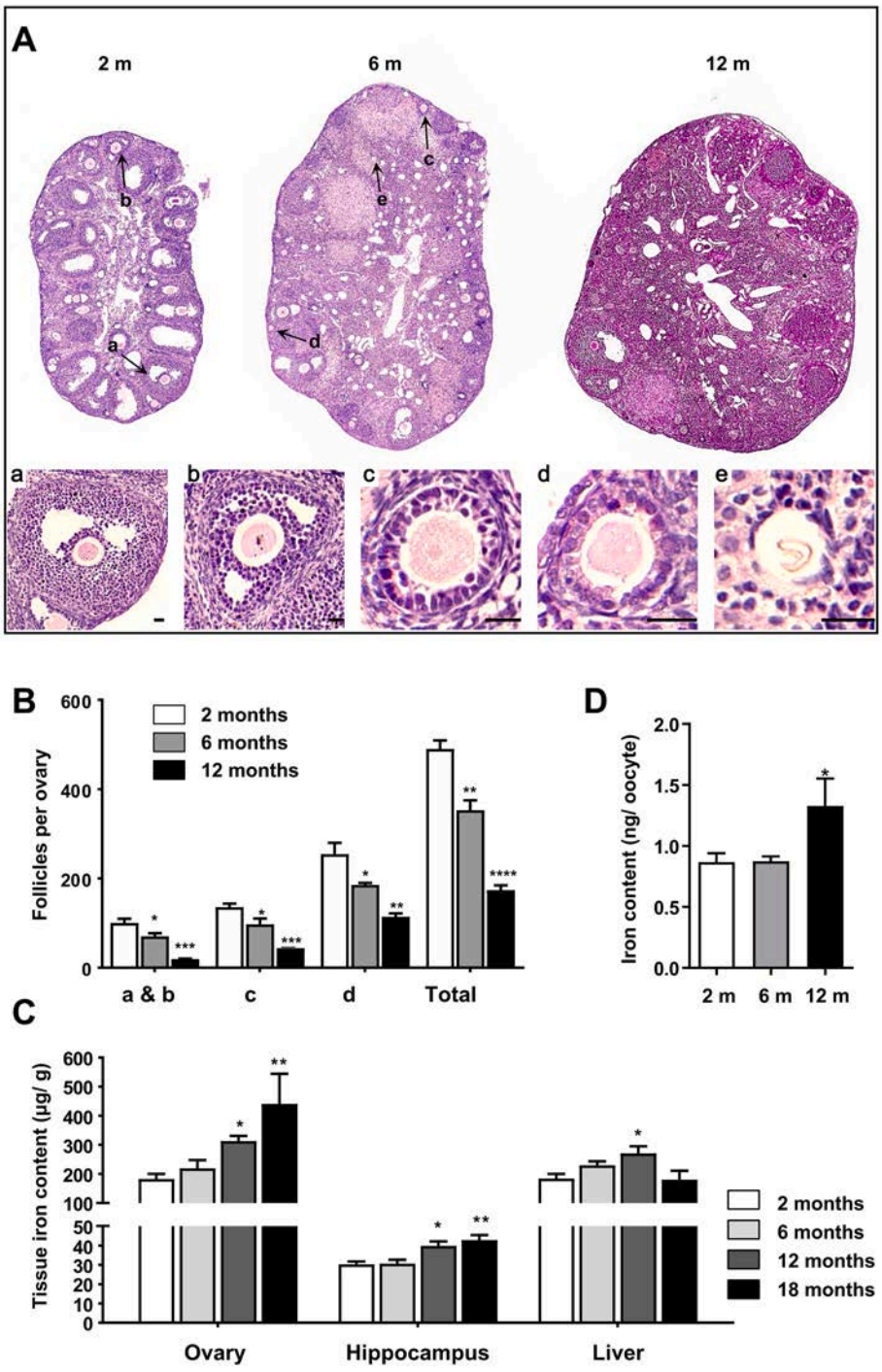

Fig. 1. The decrease in ovarian follicle number and increase in ovarian iron content during mice natural aging. The iron content in mouse ovary, hippocampus, liver and oocytes was detected by inductively coupled plasma mass spectrometry (ICP-MS). **A.** Representative images of ovarian HE staining section of 2, 6, 12 months group mice. The arrows point to: **(a).** Antral follicle; **(b).** Secondary follicle; **(c).** Primary follicles; **(d).** Primordial follicle; **(e).** Atretic follicle. (n = 3). Scale bar = 20 μm. **B.** Statistical analysis of the number of follicles at each level in ovarian HE staining section of 2, 6, 12 months group mice. **C.** Iron content per gram in ovary, hippocampus and liver in mice at age of 2, 6, 12 and 18 months. (n = 8/group). **D.** The average iron content in oocyte of mice at age of 2, 6, 12 months. (2 m: 0.8663 ± 0.07412, 6 m: 0.8736 ± 0.03956, 12 m: 1.329 ± 0.2243; n = 280/group). Data were presented as mean ± SEM of at least three times independent experiments. $^{*}P < 0.05$, $^{**}P < 0.01$, $^{***}P < 0.005$, $^{****}P < 0.001$.

remained pretty stable in oocytes at 12 months (Fig. 3C line 1–4, M − P). In addition, the level of malondialdehyde (MDA) was also significantly increased (Fig. 3 D line 1, Q), suggesting an up-regulation of lipid peroxidation in oocytes. Beyond expectation, the key antioxidant molecule mitochondrial superoxide dismutase (SOD2) [33] was up-regulated while GPX4 and Peroxiredoxin (PRX) [28] were not changed much in aging oocytes (Fig. 3 D line 2–4, R- T), it showed that the cellular antioxidant capacity was still not exhausted by ROS. What's more, the mitochondrial fusion protein mitofusin-1 (MFN1) exhibited no significant changes (Fig. 3 D line 5, U), indicating no catastrophic changes in the outer mitochondrial membrane fusion dynamics [34].

Furthermore, we observed changes in organelles changes in oocytes through live cell imaging. As illustrated by live cell imaging, the total fluorescent intensity of Fe^{2+} signal was significantly higher in aging

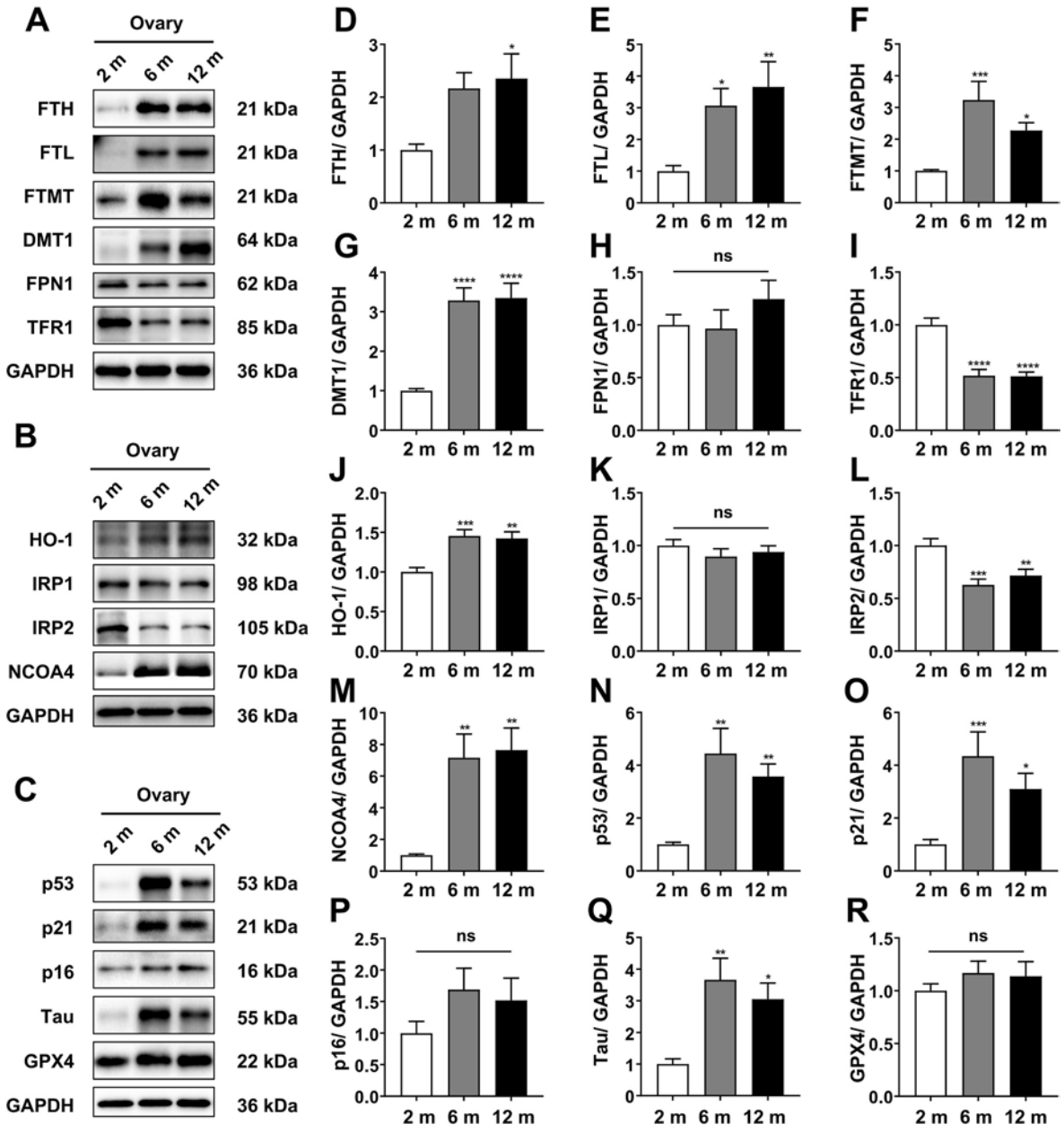

Fig. 2. Dynamic changes of iron metabolic proteins in natural aging ovaries. A. Western blot analysis of FTH, FTL, FTMT, DMT1, FPN1 and TFR1 in the ovaries from mice at age of 2, 6, 12 months. **B.** Western blot analysis of HO-1, IRP1, IRP2 and NCOA4 in the ovaries from mice at age of 2, 6, 12 months. **C.** Western blot analysis of p53, p21, p16, Tau and GPX4 in the ovaries from mice at age of 2, 6, 12 months. **D-R.** Statistical analysis of difference in protein levels of FTH, FTL, FTMT, DMT1, FPN1, TFR1, HO-1, IRP1, IRP2, NCOA4, p53, p21, p16, Tau and GPX4 in the ovaries from mice at age of 2, 6 and 12 months. (n = 8). Total proteins values were compared to the 2 months. Data were presented as mean ± SEM of at least three times independent experiments. $^{*}P < 0.05$, $^{**}P < 0.01$, $^{***}P < 0.005$, $^{****}P < 0.001$.

oocytes when labeled with FeRhonox-1 (Fig. 4 A- B). This indicates enhanced amount of free Fe^{2+} in cytosolic area, logically consistent with the higher total iron and lower FTH in aging cells. The purple Fe^{2+} signal was mainly aggregated in the area surrounding the speculative spindle and also presented as dots across the cytoplasm, and some dots were colocalized with lysosomes, which were labeled with LysoTracker probe in green. The dot-like signal of both Fe^{2+} and lysosomes were simultaneously increased in size and number in aging oocytes (Fig. 4 A, C). The colocalization feature implies the cytosolic Fe^{2+} may be mainly sourced from lysosomal breakdown of FTH along ferritinophagic flux. Fe^{2+} signal was also colocalized with mitochondria in the area around the speculative spindle, a limited number of dot-like Fe^{2+} signal was also overlapped with mitochondria in the cytoplasmic area. Obviously, in aging oocytes, mitochondrial structure is more dispersed and the number of dot- and patch-like clusters of mitochondria were increased in cytoplasm, which were overlapped by Fe^{2+} signal (Fig. 4 A, D- E). Statistics further confirmed increased Fe^{2+} signal on mitochondria and lysosome in aging oocytes (Fig. 4 F- G).

Additionally, the level of ROS, as labeled with DCFH-DA, was significantly enhanced in oocytes at 12 months, which was colocalized with the red signal of mitochondria probed with MitoTracker (Fig. 5 A-B), suggesting an up-regulation of mtROS. During JC-1 detection, the intensity ration of red/green fluorescent signal was dramatically reduced in aging oocytes (Fig. 5 C- D), clearly indicating a decrease in mitochondrial membrane potential, a landmark event in the early stage of cell apoptosis. This was further confirmed by the elevated signal of

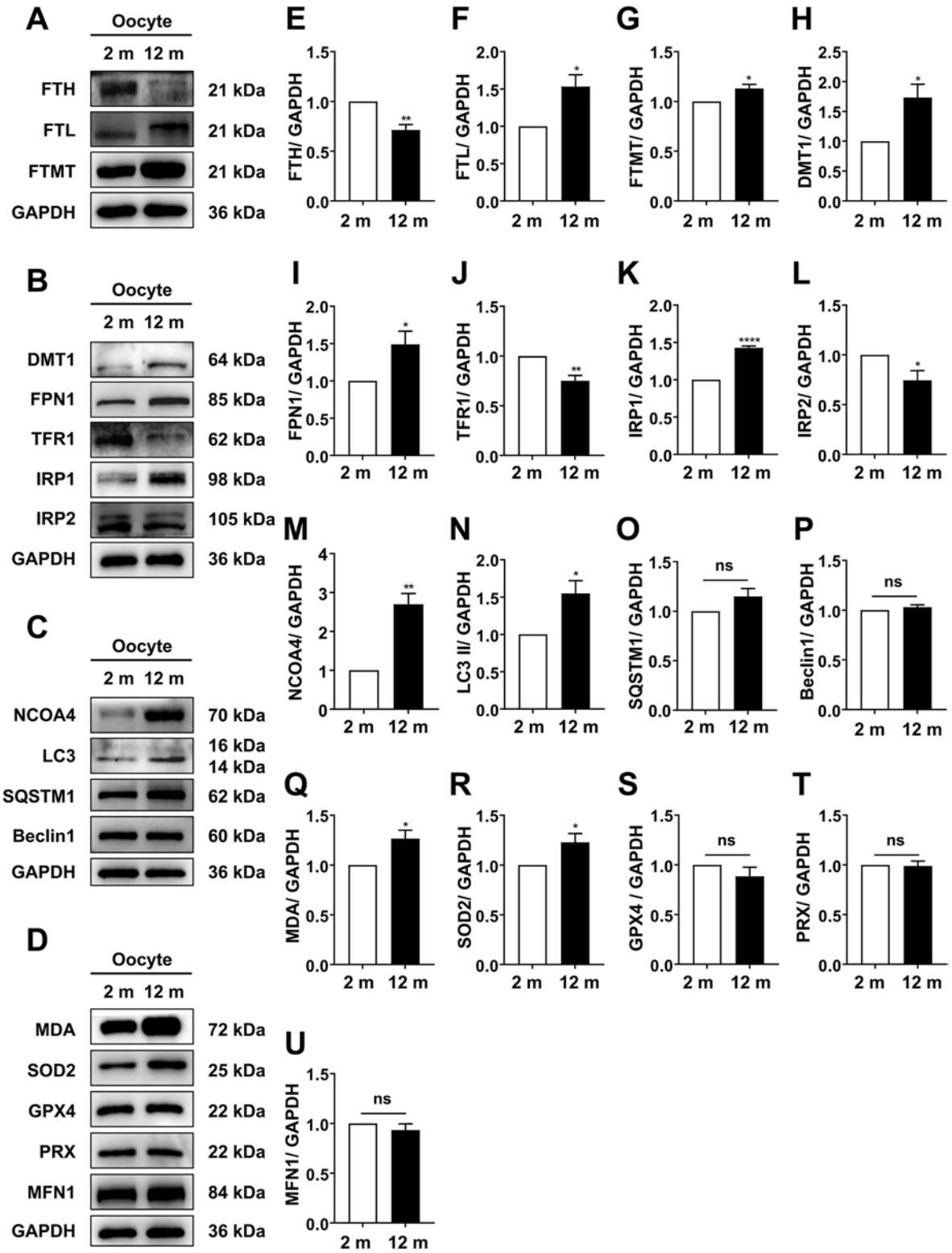

Fig. 3. Changes in protein expression relevant to iron metabolism, autophagy and oxidative stress in natural aging oocytes. A. Western blot analysis of FTH, FTL and FTMT in the oocytes from mice at age of 2 and 12 months. **B.** Western blot analysis of DMT1, FPN1, TFR1, IRP1 and IRP2 in the oocytes from mice at age of 2 and 12 months. **C.** Western blot analysis of NCOA4, LC3, SQSTM1 and Beclin1 in the oocytes from mice at age of 2 and 12 months. **D.** Western blot analysis of MDA, SOD2, GPX4, PRX and MFN1 in the oocytes from mice at age of 2 and 12 months. **E-U.** Statistical analysis of difference in protein levels of FTH, FTL, FTMT, DMT1, FPN1, TFR1, IRP1, IRP2, NCOA4, LC3 II, SQSTM1, Beclin1, MDA, SOD2, GPX4, PRX and MFN1 in the oocytes from mice at age of 2 and 12 months. (n = 3–5). Total proteins values were compared to the 2 months, which was normalized to 1.0. Data were presented as mean ± SEM of at least three times independent experiments. $^{*}P < 0.05$, $^{**}P < 0.01$, $^{****}P < 0.001$.

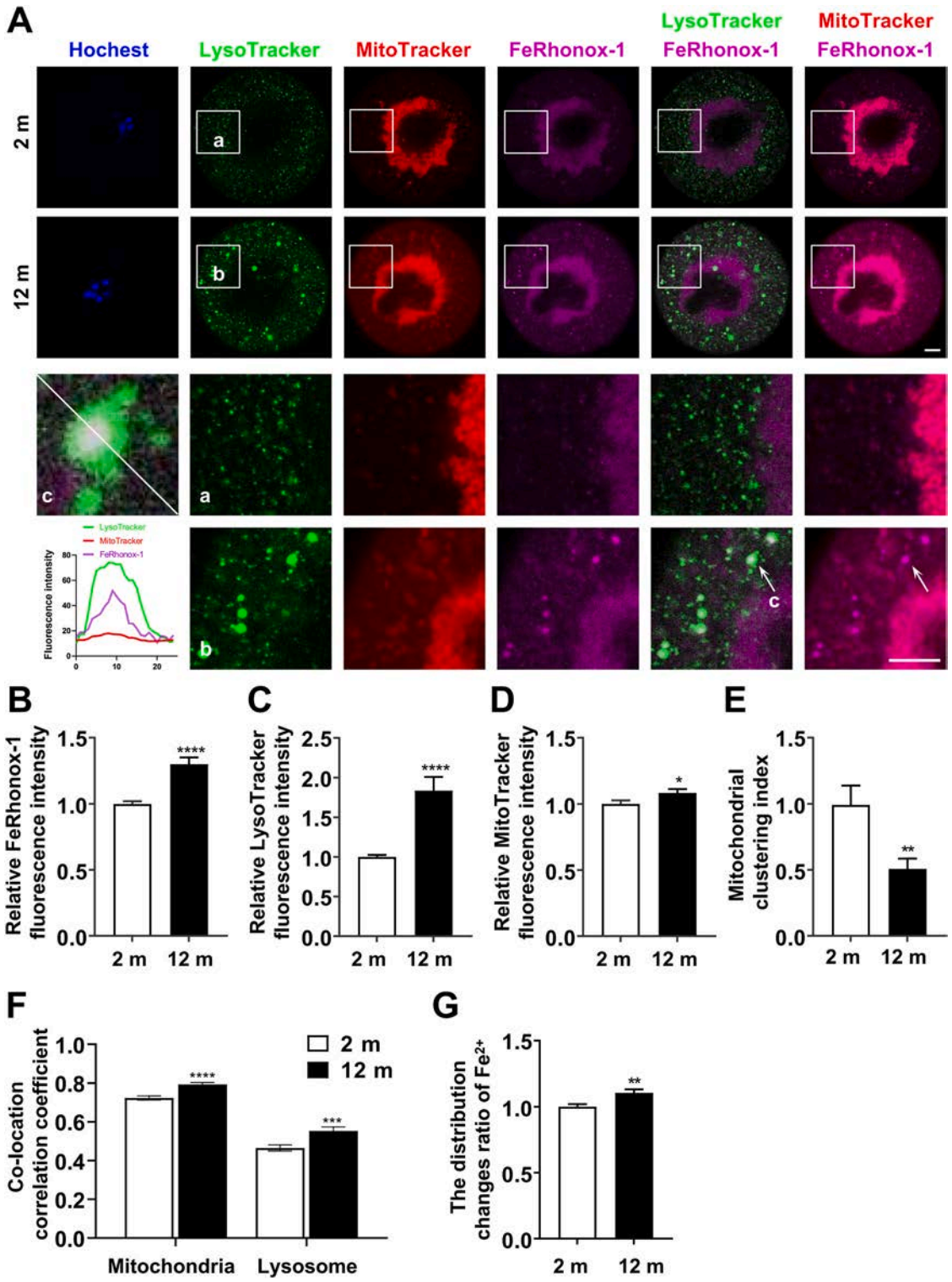

Fig. 4. Fe^{2+} accumulation in mitochondria and lysosome in aging oocytes. A. Representative images of LysoTracker, MitoTracker and FeRhonox-1 signal in the oocytes at age of 2 and 12 months. Hochest was showed in blue, Lysotracker was showed in green, Mitotracker was showed in red, FeRhonox-1 was showed in purple. **(a)** and **(b)** were enlarged diagram of marked square in representative images. **(c)** was enlarged diagram of arrow pointed coincident point in representative images. Scale bar = 10 μm. **B-D.** Relative fluorescence intensity of LysoTracker, MitoTracker and FeRhonox-1 signal in the oocytes of 2 and 12 months. (n = 35–46). **E.** Statistical analysis of mitochondrial clustering index in the oocytes of 2 and 12 months. (n = 28–29). **F.** Statistical analysis of spearman's rank correlation value (ρ) of co-location between FeRhonox-1 with LysoTracker or Mitotracker in the oocytes of 2 and 12 months. (n = 38–48). **G.** Statistical analysis of co-localization migration rate of Fe^{2+} from mitochondria to lysosomes. The formula for calculation is as follows: ρ (co-location between FeRhonox-1 and LysoTracker)/ρ (co-location between feRhonox-1 and MitoTracker). (n = 37–47). Three 2-month-old mice and six 12-month-old mice were used in this experiment. Data were presented as mean ± SEM of at least three times independent experiments. $^{*}P < 0.05$, $^{**}P < 0.01$, $^{***}P < 0.005$, $^{****}P < 0.001$.

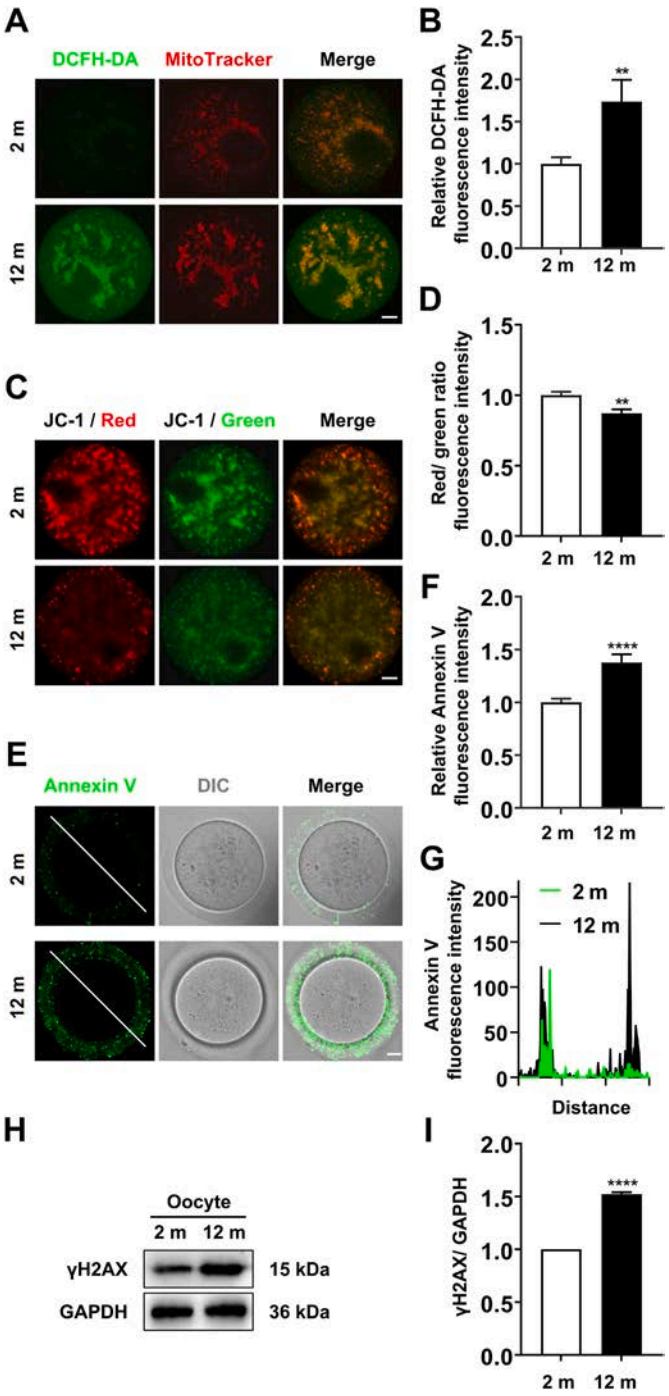

Fig. 5. The aging oocytes exhibit high ROS, early apoptosis and DNA damage. A. Representative images of DCFH-DA and MitoTracker signal in the oocytes at age of 2 and 12 months. DCFH-DA was showed in green, MitoTracker was showed in red. Scale bar = 10 μm. **B.** Relative fluorescence intensity of DCFH-DA signal in the oocytes at age of 2 and 12 months. (n = 30–36). **C.** Representative images of JC-1 signal in the oocytes at age of 2 and 12 months. JC-1/monomers were showed in green; JC-1/aggregates were showed in red. Scale bar = 10 μm. **D.** Relative fluorescence intensity of JC-1 red/green in the oocytes at age of 2 and 12 months. (n = 29–49). **E.** Representative images of Annexin V signal in the oocytes at age of 2 and 12 months. Scale bar = 10 μm. **F.** Relative fluorescence intensity of Annexin V signal in the oocytes at age of 2 and 12 months. Annexin V was showed in green. (n = 31–33). **G.** Fluorescence intensity profiling of phalloidin in representative images. Lines were drawn through the oocytes, and pixel intensities were quantified along the lines. **H.** Western blot analysis of γH2AX in the oocytes at age of 2 and 12 months. **I.** Statistical analysis of difference in protein levels of γH2AX in the oocytes at age of 2 and 12 months. Total fluorescence intensity or proteins values were compared to the 2 months. Nine 2-month-old mice and eighteen 12-month-old mice were used in this confocal experiment. Data were presented as mean ± SEM of at least three times independent experiments. $^{**}P < 0.01$, $^{****}P < 0.001$.

Annexin V across the membrane in oocytes of 12-month-old mice (Fig. 5 E– G). Western blot analysis revealed γH2AX level was significantly increased in aging cells, confirming the DNA damage was enhanced (Fig. 5 H– I).

We further conducted in vitro experiments to verify Fe^{2+} impact on oocytes. Ferrous ammonium sulfate (FAS) was used as Fe^{2+} donor [35]. GV oocytes from 2-month-old mice were incubated in 3000 μM FAS for 6 h, and then processed with fluorescent probes and live cell imaging. As showed in Fig. 6, the signal of Fe^{2+} (FeRhonox-1, purple) was pronouncedly increased across the cytoplasm in FAS-treated oocytes while

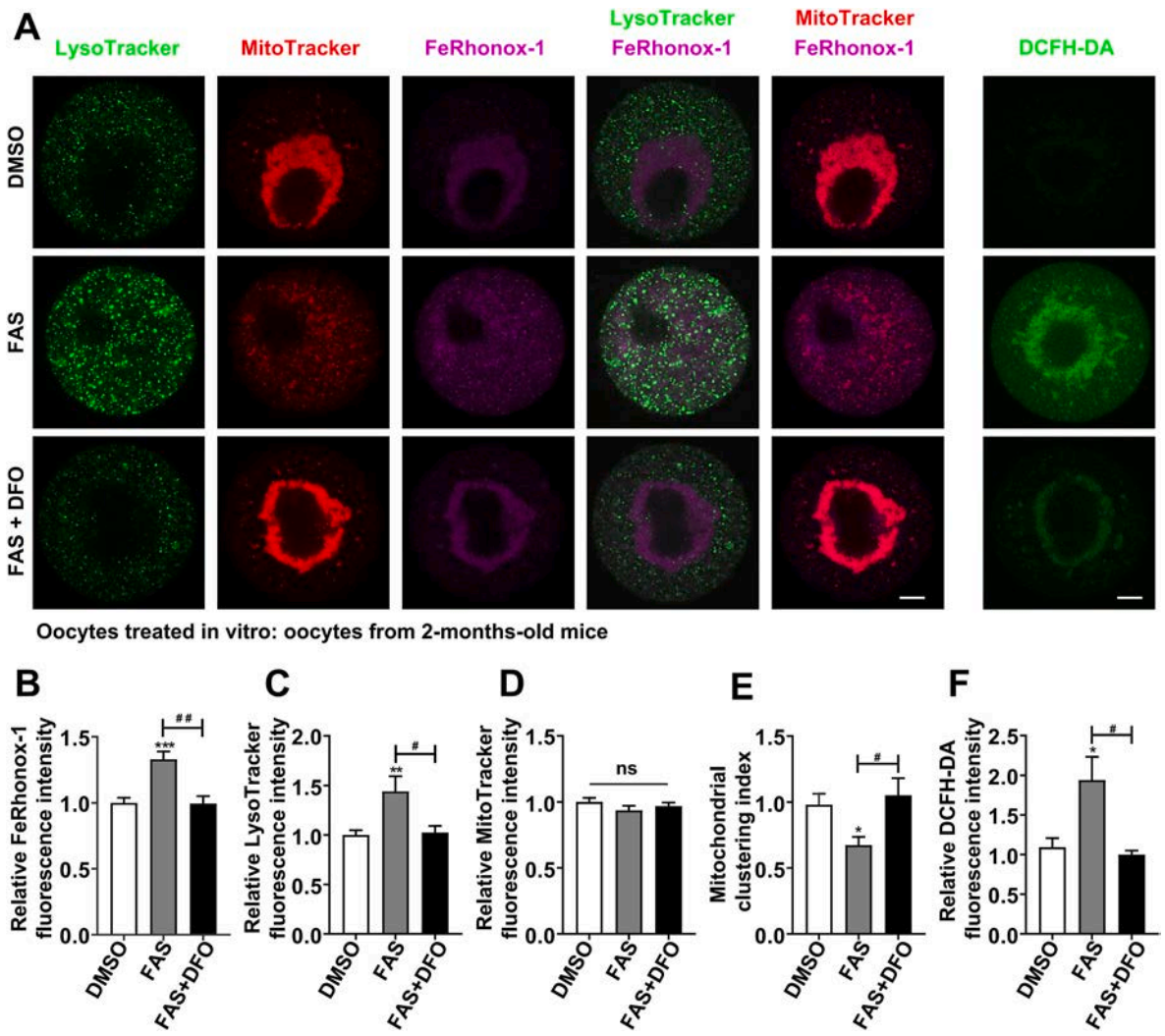

Fig. 6. Ammonium iron (II) sulfate hexahydrate (FAS) leads to an increase of Fe^{2+} and ROS in oocytes, altering the state of lysosomes and mitochondria, which could be reversed by Deferoxamine (DFO). Mice oocytes at age of 2 months were processed with the LysoTracker, MitoTracker, FeRhonox-1 and DCFH-DA staining after 6 h incubation in DMSO, 3000 μm FAS, 3000 μm FAS +3000 μm DFO. **A.** Representative images of Lysotracker, Mitotracker, FeRhonox-1 and DCFH-DA signal in the oocytes of DMSO, FAS and FAS + DFO groups. Scale bar = 10 μm. **B-D.** Relative fluorescence intensity of LysoTracker, MitoTracker and FeRhonox-1 signal in the oocytes of DMSO, FAS and FAS + DFO groups. (n = 26–34). **E.** Statistical analysis of mitochondrial clustering index in the oocytes of DMSO, FAS and FAS + DFO groups. (n = 23–32). **F.** Relative fluorescence intensity of DCFH-DA signal in the oocytes of DMSO, FAS and FAS + DFO groups. (n = 38–44). Relative fluorescence intensity was compared to the DMSO group. Twelve 2-month-old mice were used in this experiment. Data were presented as mean ± SEM of at least three times independent experiments. $^{*/\#}P < 0.05$, $^{**/\#\#}P < 0.01$, $^{***}P < 0.005$.

it was moderate and mainly confined within the area of the suggestive spindle in control cells (Fig. 6 A, B). FAS incubation did not change the overall intensity of mitochondria signal (MitoTracker, red) in oocytes, but significantly decreased the mitochondrial population clustering in the spindle area, however increased the portion of dot-like mitochondrial aggregates in the cytoplasmic area, and notably, mitochondrial dots were colocalized by Fe^{2+} signal (Fig. 6 A, D, E). Moreover, FAS also increased the signal intensity of lysosomes, which were aggregated as dots in different size across the cytoplasm (LysoTracker, green) (Fig. 6 A, C). The fluorescence intensity of DCFH-DA was apparently enhanced in FAS-treated oocytes (Fig. 6 A, F). As expected, all the FAS-induced changes could be properly reversed by a combined application of DFO, the iron chelating agent (Fig. 6A–F). In line with the above results, when oocytes from 12-month-old mice were cultured in DFO for 6 h, the levels of cytosolic Fe^{2+}, ROS and Annexin V signal were significantly decreased (Fig. 7 A- E), additionally, MII rate and spindle morphology were also improved (Fig. 7 F– I). In general, these data indicate the free cytosolic Fe^{2+} excessively accumulates in aging oocytes and may induce the oxidative stress and lipid peroxidation through Fenton reaction [36].

3.4. Alleviation of age-related Fe^{2+} accumulation and iron metabolism imbalance with DFO

Because DFO can in vitro correct Fe^{2+} effects in oocytes, its effects were further in vivo investigated in 12-month-old mice. As showed by the ICP-MS results in Fig. 8A, after intraperitoneal injection of DFO for 14 consecutive days, the ovarian iron content was significantly reduced in DFO treatment group than the control, which were injected with same volume of PBS. Western blot analysis demonstrated the protein levels of FTH, FTL and FTMT were effectively subsided in DFO group, especially that of FTH (Fig. 8 B, F– H). In contrast, the expression of IRP1 and IRP2 were dramatically increased, with particularly sharp rise in IRP2 (Fig. 8C line 1–2, I- J). Interestingly, no significant changes were detected in DMT1, TFR1 and FPN1 expression after DFO treatment (Fig. 8C line 3–5, K- M). The expression of NCOA4 was pronouncedly decreased (Fig. 8 D line 1, N), implying its binding to FTH is reduced. The autophagic protein LC3 II was significantly increased while Beclin1 and SQSTM1 showed no significant difference between DFO and control group (Fig. 8 D line 2–4, O- Q), suggesting up-regulated autophagic flux

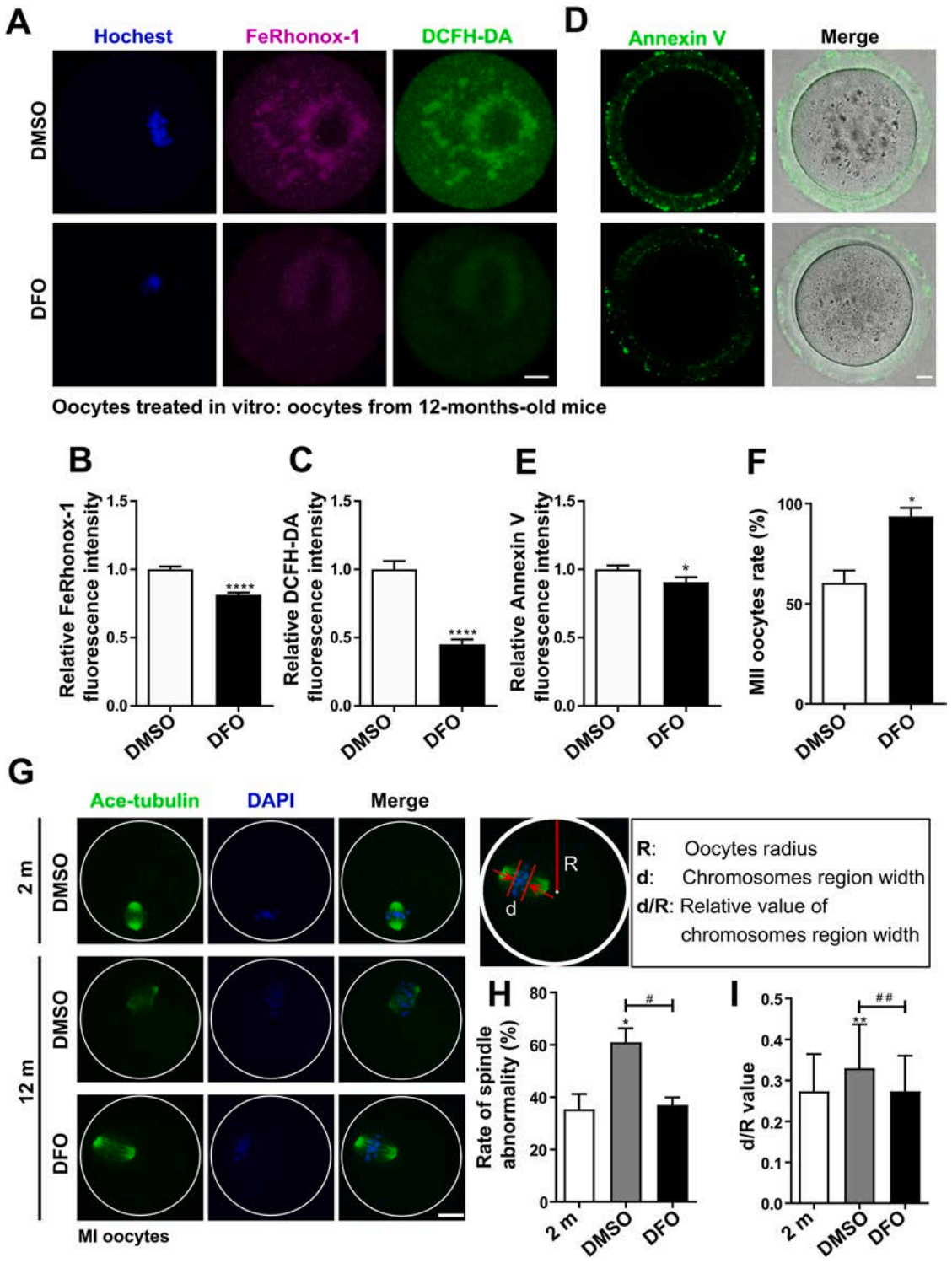

Fig. 7. Amelioration on free Fe^{2+}, ROS level and degenerative changes in aging oocytes incubated with DFO. GV oocytes were collected from mice at age of 12 months, and cultured in DMSO or 3000 μm DFO for 6 h, then processed with live imaging with FeRhonox-1, DCFH-DA and Annexin V or fixation for immunofluorescence staining. Some oocytes were cultured for 16 h in DMSO or 3000 μm DFO and collected for meiotic maturation analysis. **A.** Representative images of FeRhonox-1 and DCFH-DA signal in the oocytes of DMSO and DFO groups. Scale bar = 10 μm. **B–C.** Relative fluorescence intensity of FeRhonox-1 and DCFH-DA signal in the oocytes of DMSO and DFO groups. (n = 45–60). **D.** Representative images of Annexin V signal in the oocytes of DMSO and DFO groups. Scale bar = 10 μm. **E.** Relative fluorescence intensity of Annexin V signal in the oocytes of DMSO and DFO groups. (n = 42–44). **F.** Statistics of the rate of oocytes matured to MII phase after 16 h incubation in DMSO and DFO. **G.** Representative images of spindle in the oocytes of 2 m, 12 m- DMSO and 12 m- DFO group. The calculation model of the relative width of chromosome plate region. The radius of the oocyte is represented as R; the width of the chromosome plate is represented as d. The relative chromosomes region width = d/R. Scale bar = 10 μm. **H.** Statistical analysis of the abnormal rate of spindle in the oocytes from different groups. (n = 55–58). **I.** Statistical analysis of the d/R value of spindle in the oocytes from different groups. (n = 55–58). Relative fluorescence intensity was compared to the 12 m- DMSO. Fifteen 12-month-old mice were used in this confocal experiment. Data were presented as mean ± SEM of at least three times independent experiments. $^{*/\#}P < 0.05$, $^{**/\#\#}P < 0.01$, $^{****}P < 0.001$.

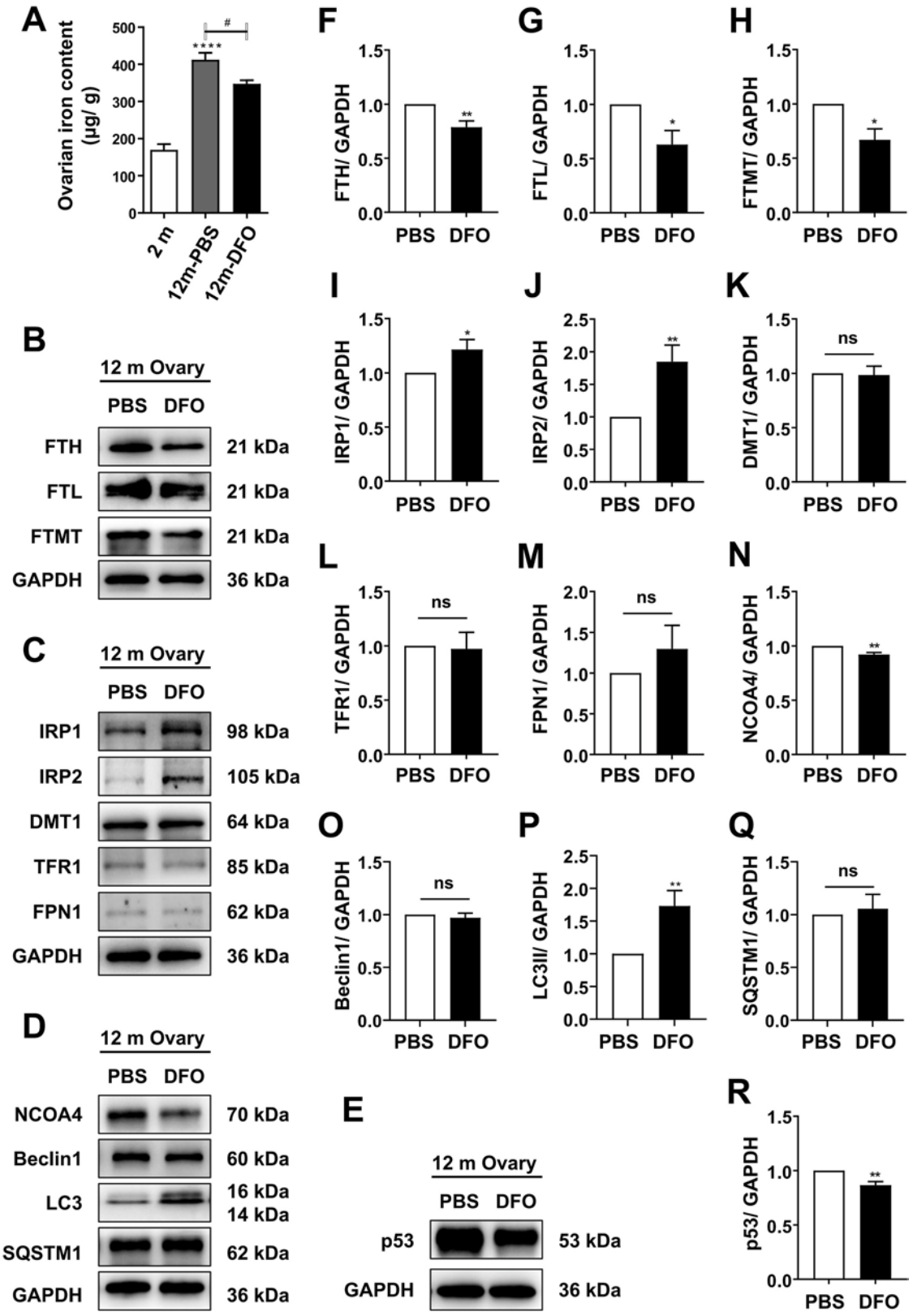

Fig. 8. DFO can rectify iron content and the expression of iron regulatory and autophagy related proteins in the ovaries of aging mice. The 12 months mice were injected intraperitoneally with DFO for 14 days, while the control group was injected with PBS. **A.** Iron content per gram in the ovaries of 2 m, 12m- PBS and 12m-DFO group. (2 m: 170 ± 15.33, 12 m-PBS: 412.4 ± 18.48, 12 m-DFO: 347.7 ± 9.666; n = 7/group). **B.** Western blot analysis of FTH, FTL and FTMT in ovaries of PBS and DFO group. **C.** Western blot analysis of IRP1, IRP2, DMT1, TFR1 and FPN1 in the ovaries of PBS and DFO group. **D.** Western blot analysis of NCOA4, Beclin1, LC3, and SQSTM1 in ovaries of PBS and DFO group. **E.** Western blot analysis of p53 in the ovaries of PBS and DFO group. **F–R.** Statistical analysis of difference in protein levels of FTH, FTL, FTMT, IRP1, IRP2, DMT1, FPN1, TFR1, NCOA4, Beclin1, LC3 II, SQSTM1 and p53 in the ovaries of PBS and DFO group. (n = 5–8). Total proteins values were compared to the PBS group, which was normalized to 1.0. Data were presented as mean ± SEM of at least three times independent experiments. $^{*}P < 0.05$, $^{**}P < 0.01$.

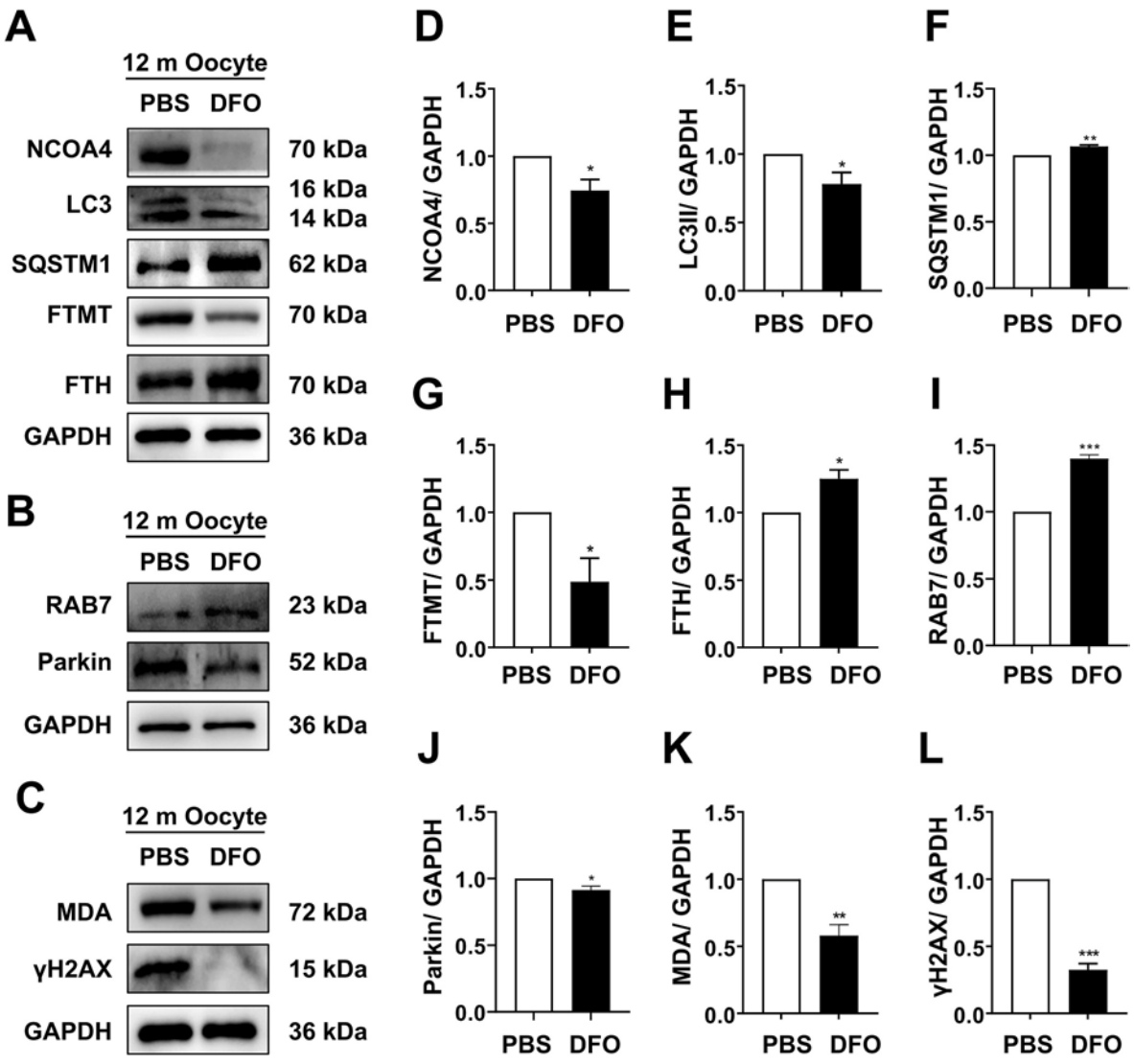

Fig. 9. DFO can correct ferritinophagy, mitophagy and oxidative stress in aging oocytes. The 12 months mice were injected intraperitoneally with DFO for 14 days, while the control group was injected with PBS. **A.** Western blot analysis of NCOA4, LC3, SQSTM1, FTMT and FTH in the oocytes of PBS and DFO group. **B.** Western blot analysis of RAB7 and Parkin in the oocytes of PBS and DFO group. **C.** Western blot analysis of MDA and γH2AX in the oocytes of PBS and DFO group. **D-L.** Statistical analysis of difference in protein levels of NCOA4, LC3, SQSTM1, Parkin, RAB7, FTMT, FTH, MDA and γH2AX in the oocytes of PBS and DFO group. (n = 3–4). Total proteins values were compared to the PBS group, which was normalized to 1.0. Data were presented as mean ± SEM of at least three times independent experiments. $^{*}P < 0.05$, $^{**}P < 0.01$, $^{***}P < 0.005$.

in DFO-treated ovaries. The protein level of p53, the key inducer of organismal aging, was substantially decreased in ovaries after DFO administration (Fig. 8 E, R). Together, the ICP-MS and Western blot analysis indicate DFO application can effectively reduce the iron accumulation, and simultaneously call back the compensatory changes in iron metabolic regulatory proteins in ovaries of 12-month-old mice.

In vivo DFO treatment also induced a shift of protein expression in oocytes. As showed in Fig. 9, NCOA4 was apparently reduced in oocytes from 12-month-old mice with DFO injection (Fig. 9 A line 1, D), at the same time, LC3 II was significantly decreased while SQSTM1 and FTH were elevated (Fig. 9 A line 2–5, E– H). Here, it can say that the ferritinophagic flux is in low activity after DFO treatment, inducing the return of FTH level. In contrast to FTH, the level of FTMT was decreased in DFO oocytes (Fig. 9 A line 4, G), indirectly implying a weakened need for mitochondria membrane to take over free Fe^{2+} after iron chelating by DFO. In addition, the protein level of RAB7 was up-regulated while that of Parkin was down-regulated (Fig. 9 B, I-J), this shows that Parkin-mediated mitophagy pathway is inhibited, maybe due to an increase in RAB7 activity, and thus reducing mitochondria damage in oocytes [37]. Concurrently, lipid peroxidation and DNA damage were also alleviated by DFO, as indicated by the decrease of MDA and γH2AX in oocytes (Fig. 9C, K- L).

3.5. Amelioration of fertility by DFO treatment

As showed in Fig. 10, ovary follicle development and survival were examined with HE staining after DFO treatment in 12-month-old mice. Compared to control group, the number of follicles, including primordial follicles, primary follicles, secondary follicle and antral follicle, was significantly higher in DFO group (Fig. 10 A- B). Meanwhile, the serum level of AMH was also higher in DFO group than control (Fig. 10C). These results suggest the decline in ovarian reserve was effectively delayed. Of course, the protective ability of DFO is limited, the number of follicles at different stages in the DFO group was still much lower than the 6-month-old mice (Table 2 in supplement).

Consistent with the ICP-MS results, the prussian blue staining revealed that the level of hemosiderin deposition was markedly elevated in ovaries from 12-month-old mice, and could be greatly lowered down

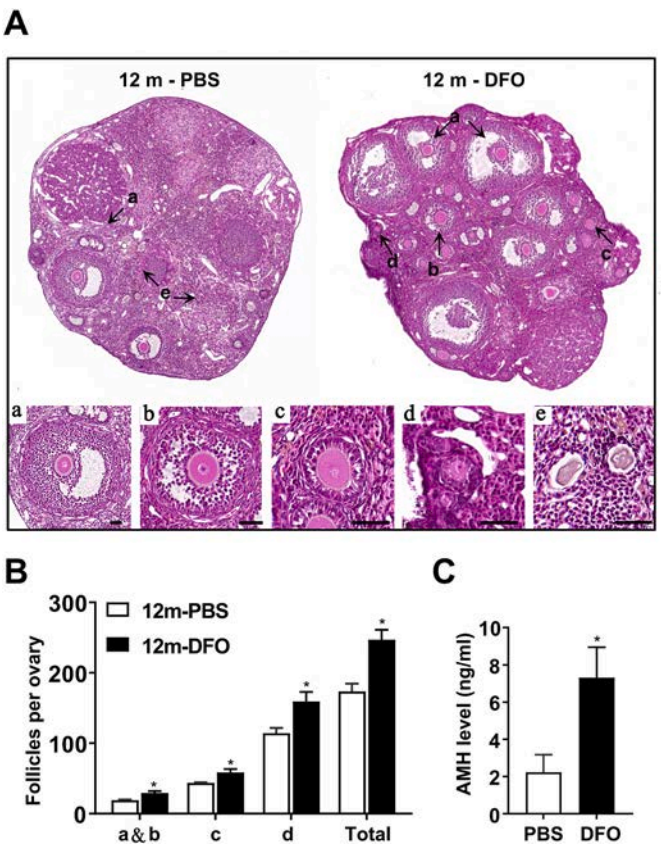

Fig. 10. DFO can delay the decline of ovarian reserve in aging mice. The 12 months mice were injected intraperitoneally with DFO for 14 days, while the control group was injected with PBS. **A.** Representative images of ovarian HE staining section of PBS and DFO group mice. The arrows point to: **(a).** Antral follicle; **(b).** Secondary follicle; **(c).** Primary follicles; **(d).** Primordial follicle; **(e).** Atretic follicle. (n = 3–4). Scale bar = 50 μm. **B.** Statistical analysis of the number of follicles at each level in ovarian HE staining section of PBS and DFO group mice. **C.** Statistical analysis of AMH content in serum of PBS and DFO group mice. (n = 6/group). Data were presented as mean ± SEM of at least three times independent experiments. $^{*/\#}P < 0.05$, $^{****}P < 0.001$.

by DFO administration (Fig. 11 A- B). As demonstrated by Masson staining, there were obvious fibrotic changes in aging ovaries, which was also alleviated after in vivo treatment with DFO (Fig. 11 C- D). Immunohistochemical analysis illustrated the application of DFO in vivo could diminish the accumulation of 4-HNE and 8-OHdG, the oxidative damage products, in the aging ovarian stroma (Fig. 11 E– H).

As indicated with live cell fluorescent imaging and statistical analysis, the fluorescent intensity of intracellular Fe^{2+} signal was dramatically lowered (Fig. 12 A, C), simultaneously, lysosome abundance was also sharply reduced (Fig. 12 A, D), and the proportion of abnormal mitochondria distribution was decreased in DFO oocytes (Fig. 12 A, E–F). In addition, the co-localization of Fe^{2+} and lysosomes also decreased in DFO oocytes (Fig. 12 G- H). In line with the reduction in cytosolic free Fe^{2+} level, the intensity of ROS probe DCFH-DA was apparently decreased (Fig. 12 B, I), and mitochondrial membrane potential index, the ratio of JC-1 red signal to green signal, was significantly elevated (Fig. 12 B, J), as well as the index of early apoptosis, as labeled with Annexin V-FITC, was dramatically diminished (Fig. 12B–K).

Logically consistent with the above data, the number of MII oocytes, retrieved after superovulation, was increased significantly in DFO group, and simultaneously, the fragmentation rate was decreased dramatically (Fig. 13 A- C). Further, as illustrated by staining on chromosome spreads, abnormal chromosome morphology, especially chromosome compacting, was less frequently observed in DFO group compared to control (Fig. 13 G, I). The chromosome counting of MII oocytes, only including the countable chromosome samples, demonstrated the aneuploid rate was markedly lower in DFO group (Fig. 13 G, H). The egg aneuploidy is mainly due to chromosome separation errors in meiosis I, and usually associated with defects in MI spindle apparatus. As the immunofluorescence showed, the abnormal spindles were frequently observed in MI oocytes from 12-month-old mice, when compared to that from 2-month-old mice. As expected, the proportion of abnormal spindles could be greatly reduced by DFO application, that is, the defects in microtubule density, spindle long axis length and bipolarity, as well as the chromosomes alignment, were all perfectly rectified (Fig. 13 D- F).

According to the above results, it may be safe to assume that in vivo application of DFO effectively reduced the cytosolic Fe^{2+} in oocytes, specifically by weakening ferritinophagy, and alleviated the oxidative stress toxicity on oocytes.

4. Discussion

This study demonstrated that the impairment in iron metabolism regulatory system induces excessive iron accumulation in mouse aging ovaries, leading to ferrous iron superfluity and subsequently, oxidative stress and degenerative changes in oocytes, and ultimately the decline in ovarian reserve. In vivo iron chelating can delay ovary reserve decline and ameliorate oocyte degeneration.

Ovarian aging is classically considered the main cause of female reproductive infertility, and mainly due to the imbalance in active oxygen metabolism, involving a complex and multifaceted process [38]. Fe^{2+} forms cytoplasmic labile iron pool (LIP) which acts as an intermediate between imported, stored, and utilized iron, and is critical for iron homeostasis maintenance [39]. In cellular physiological activities, Fe^{2+} is used as the carrier to deliver oxygen by participating in the Fenton reaction, and the byproduct of this process is hydroxyl radical. Hyperactive Fenton reaction surely produces redundant hydroxyl radical, thereby causes oxidative damage, lipid peroxidation, and thus tissue injury [40]. As in oocytes, excessive hydroxyl radical seriously damages the spindle microtubules and chromosome alignment [41,42]. In humans, multiple organs including the liver, kidney, and brain show age-related iron accumulation [9], and some neurodegenerative pathogenesis, such as Alzheimer's disease, are closely correlated with iron overload in the aging brain [43]. Till now, there have been some studies which report age-related accumulation of non-heme ferric iron and Fe^{2+} in mouse ovary, but much less attention has focused on the changes in iron homeostasis regulatory mechanism in aging ovaries or oocytes [44,45]. In our study, we found a rising trend in the iron content per unit mass of ovary, hippocampus and liver in aging mice, remarkably, the degree of iron increase was higher in ovary than in hippocampus and liver. This may be due to the ovary is a highly vascularized organ [1,40,46]. The ovaries experience periodic events of follicle development, rupture, ovulation and luteinization during female reproductive life span, that means repeated cycles of angiogenesis and bleeding [1,40,47], and thereby continuous accumulation of erythrocyte degradation products. As a support for this assumption, we detected an increased hemosiderin deposition and HO-1 expression in ovarian tissue of aging mice, this implies constant and high iron release from heme decomposition [48]. For human, women's menstrual cycle represents another substantial hemoglobin lysis in the uterus, so the pelvic cavity, which embraces the ovaries, is also an iron-rich microenvironment [49]. Previous studies have showed that the increase in free iron of patients with endometriosis promotes oxidative stress through the Fenton reaction, leading to infertility [50]. It may be right that the follicular granulosa cells and oocytes are exposed to continuous ferrous iron from heme breakdown along with the age [45].

It has been evidenced that HO-1 upregulation is associated with neurotoxic iron deposition in aging and age-related diseases [19],and the genetic or chemical inhibition of HO-1 could induce apparent

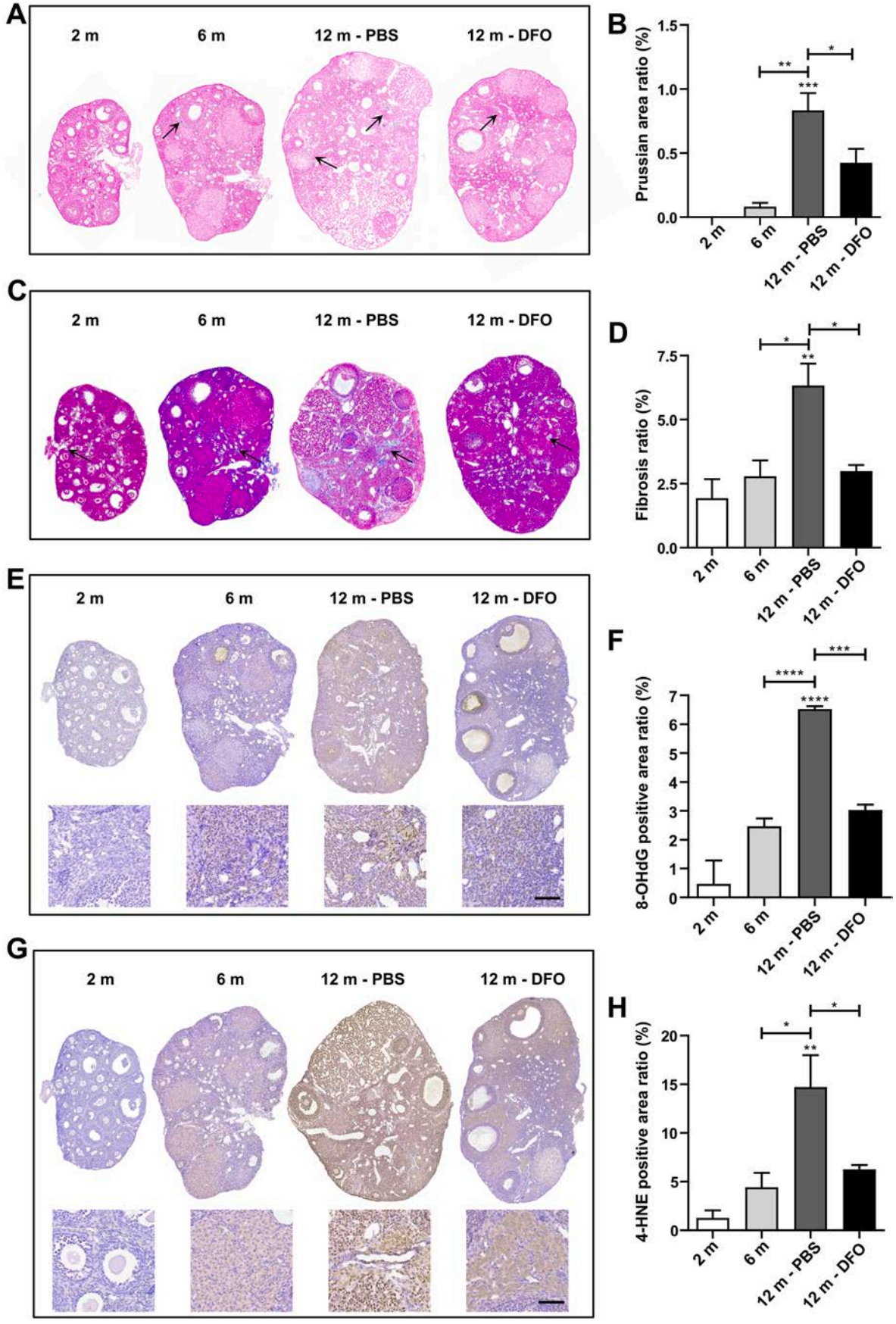

(caption on next page)

Fig. 11. DFO can reduce the levels of iron accumulation, fibrotic changes, and 8-OHdG and 4-HNE in aging ovaries. The 12 months mice were injected intraperitoneally with DFO for 14 days, while the control group was injected with PBS. **A.** Representative images of Prussian blue staining in ovary sections of 2 m, 6 m, 12 m- PBS and 12 m- DFO group mice. **B.** Statistical analysis of the intensity of Prussian blue signal in ovary sections of 2 m, 6 m, 12 m- PBS and 12 m- DFO group mice. **C.** Representative images of Masson staining in ovary sections of 2 m, 6 m, 12 m- PBS and 12 m- DFO group mice. **D.** Statistical analysis of the intensity of Masson signal in ovary sections of 2 m, 6 m, 12 m- PBS and 12 m- DFO group mice. **E.** Representative images of 8-OHdG immunohistochemical staining in ovary sections of 2 m, 6 m, 12 m- PBS and 12 m- DFO group mice. **F.** Statistical analysis of 8-OHdG level in ovary sections from different groups. **G.** Representative images of 4-HNE immunohistochemical staining in ovary sections of 2 m, 6 m, 12 m- PBS and 12 m- DFO group mice. **H.** Statistical analysis of 4-HNE level in ovary sections from different groups. This portion of the experiment involved sectioning and staining wax blocks prepared from one side of the ovaries of three different mice. Specifically, the statistical approach involved serially sectioning approximately 45 slices near the largest surface of the mouse ovary. Every 15th slice was chosen for staining and statistical analysis. The average of the statistical results from three selected slices represented the proportion of positive staining or antibody expression area in the ovary. Finally, statistical analysis was performed on the results from the three mice. Data were presented as mean ± SEM of at least three times independent experiments. $^{*}P < 0.05$, $^{**}P < 0.01$, $^{***}P < 0.005$, $^{****}P < 0.001$.

improvement in iron status and degenerative alterations in aging mice [43]. Similarly, the increase in ovarian HO-1 expression and iron content may be also associated with degenerative changes in aging ovaries, such as follicular atresia, ovarian fibrosis and cell cycle arrest. But cannot be ignored is that HO-1, with its ability to reverse oxidative damage and stress, has also been proved to play critical roles in antioxidant defense and various pathophysiologic processes in an age-related manner [51,52]. Therefore, it is highly necessary to further explore whether HO-1 can be targeted for intervention strategy on ovarian aging.

Iron exists in two forms: heme and non-heme. Heme iron is degraded into Fe^{2+} by HO-1, the released Fe^{2+} is transported into the cytoplasm through DMT1 and incorporated into the labile iron pool [53]. Non-heme iron binds to TFR1 and enters the cell through endocytosis, and is transported to the lysosomes where Fe^{3+} ions dissociate from TFR1 and are reduced back to Fe^{2+} ions, then incorporated into the labile iron pool by DMT1 [9]. In our study, we found that the protein expressions of above iron regulators were changed in mouse aging ovaries. TFR1 was decreased in both ovaries and oocytes, this reduction suggests, combined with HO-1 increase, the main source of ovarian iron may be from heme degradation after puberty, and properly not from serum non-heme source [22]. In contrast, the level of DMT1 and FPN1 was elevated in ovaries and oocytes, this indicates active intracellular Fe^{2+} release and transporting, also an increasing iron export. The expressions of three iron storage proteins, FTH, FTL and FTMT, were also ascended in aging ovaries. Ferritin members, especially FTH, work to reduce iron from ferrous to ferric, and store it in a non-oxidizing active state [16,38]. Their upregulation may suggest an increasing antagonistic mechanism to sequester Fe^{2+} in the ovarian microenvironment. Consistently, these changes are in line with decreased levels of IRP2 in aging ovaries and oocytes. It was previously showed that IRP2 can increase the translational expression of TRF1, and simultaneously decrease the expression of FTH, FTL, FTMT and DMT1, so as to upregulate iron uptake, and meanwhile downregulate iron storage [18]. Therefore, IRP2 reduction may be specific response to iron accumulation in aging ovaries, attempting to increase iron storing. Here we can conclude that all these regulators coordinate to balance the iron homeostasis in condition of iron rise, which may be derived from HO-1 catabolism. Although the body actively responds to the increase in iron, the imbalance of iron homeostasis ultimately leads to oxidative stress in aging ovaries [1]. Here we found the signal intensity of MDA, 4-HNE and 8-OHdG was increased in aging ovaries, which was also accompanied with upregulated expression of p21, p16, Tau and p53, suggesting an increasing trend in lipid peroxidation and oxidative DNA damage, as well senescence traits in ovaries [54].

NCOA4 is a cargo protein able to promote selective autophagic ferritin degradation, essential for maintaining intracellular and systemic iron homeostasis [55]. Current evidences have proved that NCOA4 upregulation is associated with iron redundance in aging brains of mice [56,57], additionally, it's over expression is also reported in aging ovaries of mice and human [58]. The increasing NCOA4 is supposed to hijack the newly synthesized FTH, reducing the portion of FTH for buffering Fe^{2+}, thereby boosting the labile iron pool in cytoplasm [59]. In line with previous reports, we detected enhanced expression of NCOA4 in aging ovaries and oocytes of mice. Interestingly, NCOA4 elevation was not responded by FTH downregulation in the whole ovarian tissue, instead these two proteins were simultaneously increased. Actually, such change pattern is also found in aging brain, and may be due to the non-immediate degradation of NCOA4-FTH complex by the dysfunctional autophagy process [57]. In contrast, high NCOA4 and LC3-II, and simultaneously low FTH, were detected in aging oocytes, this means the NCOA4-mediated ferritinophagy is active and promotes FTH degradation, which is supposed to release more Fe^{2+} into the cytosolic area. As expected, Fe^{2+} signal was increased in cytoplasm and mainly labeled on the lysosomes, which were also hyperactive, further supporting active Fe^{2+} release from FTH degradation by lysosomes. Unlike FTH, the other two iron storing proteins, FTL and FTMT, were not decreased but increased significantly in aging oocytes, that may be because FTL has lower affinity for NCOA4 [60], or these two ferritins compensate for the loss of FTH.

As the major iron transporter, DMT1 is initially identified in intestinal cells, enabling dietary iron uptake in the duodenum [30]. Recently, a differentially spliced DMT1 isoform is validated in most peripheral tissues, which is expressed at the cell surface and in endosomes, facilitates transferrin-independent iron uptake [61]. An iron challenge can trigger the internalization of apical membrane DMT1, and the intracellular ROS produced during iron uptake is also instrumental in inducing DMT1 internalization. Preincubation with the hydroxyl radical scavengers could block iron-induced endocytosis of DMT1 [62]. Importantly, the post-transcriptional expression of *Dmt1* is not just regulated by IRP alone, as proved, the IRP-independent DMT1 upregulation is apparent during aging in the central nervous system, and can be induced by inflammation and neurotoxic stimuli in primary rat hippocampal neurons. Altered DMT1 expression leads to iron deposition in neuronal cells and neurodegenerative disorder [61,62]. In the present study, we identified DMT1 expression in mouse oocytes for the first time, which has been previously validated only in *Xenopus* oocytes [63,64]. Noteworthily, the protein level of DMT1 was elevated in aging ovaries and oocytes, such elevation may contribute to, at least partially, the redundancy of cytosolic Fe^{2+} in oocytes. Perhaps similar to nerve cells, DMT1 upregulation in aging oocytes is in response to the increase of extracellular iron and intracellular ROS production via the Fenton reaction [61]. Concurrent with the rise in DMT1 and cytosolic Fe^{2+} was the elevation in FPN1 expression in aging oocytes, arguably, FPN1 increase may try to mobilize more iron out of oocytes.

During ferritinophagy, the mitochondrial membranes serve as a temporary buffer to accept Fe^{2+} from lysosome digestion of FTH [7]. In line with this assumption, we noticed that the Fe^{2+} signal was increased on mitochondria in aging oocytes. However, excess Fe^{2+} is supposed to exceed the buffering capacity of mitochondria, so the redox-active iron produces highly reactive hydroxyl radical via the Fenton reaction on the local lipid membranes, and inevitably induces oxidative stress, as illustrated by mitochondrial injury and membrane potential decline. Thereby the energy supply and Fe^{2+} buffering by mitochondria may fall further, and in turn causing more free cytosolic Fe^{2+} and cellular oxidative stress with increased lipid peroxidation, protein and nucleic

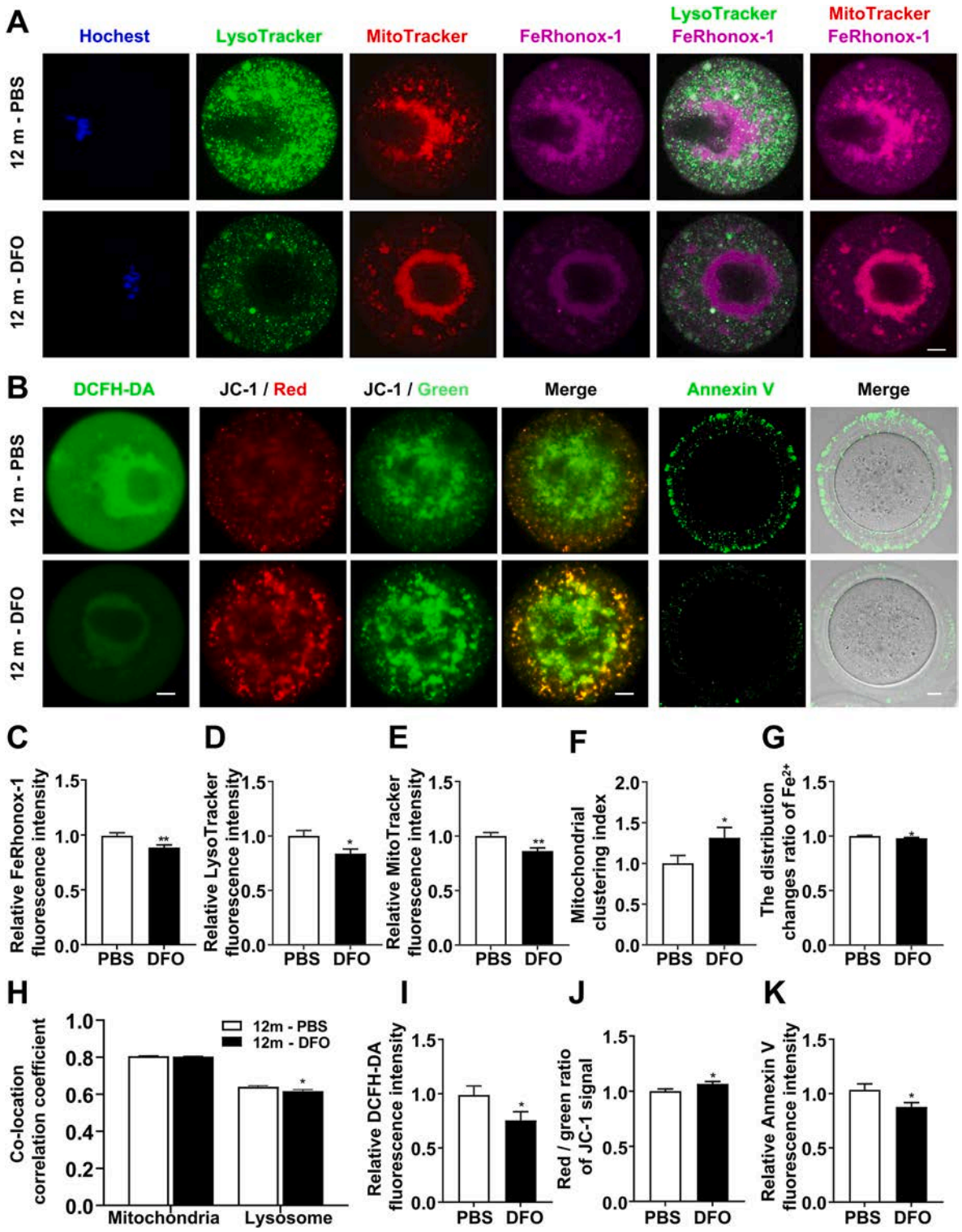

Fig. 12. DFO can alleviate the levels of free Fe^{2+}, ROS, apoptosis, and also changes in lysosome and mitochondria in aging oocytes. The 12 months mice were injected intraperitoneally with DFO for 14 days, while the control group was injected with PBS. **A.** Representative images of LysoTracker, MitoTracker and FeRhonox-1 signal in the oocytes of PBS and DFO group. Scale bar = 10 μm. **B.** Representative images of DCFH-DA, JC-1 and Annexin V signal in the oocytes of PBS and DFO group. Scale bar = 10 μm. **C-E.** Relative fluorescence intensity of LysoTracker, MitoTracker and FeRhonox-1 signal in the oocytes of PBS and DFO group. (n = 44–62). **F.** Statistical analysis of mitochondrial clustering index in the oocytes of PBS and DFO group. (n = 35–39). **G.** Statistical analysis of spearman's rank correlation value (ρ) of co-location between FeRhonox-1 with LysoTracker or MitoTracker in the oocytes of PBS and DFO group. (n = 42–49). **H.** Statistical analysis of co-localization migration rate of Fe^{2+} from mitochondria to lysosome. The formula for calculation is as follows: ρ (co-location between FeRhonox-1 and Lysotracker)/ρ (co-location between FeRhonox-1 and Mitotracker). (n = 44–49). **I.** Relative fluorescence intensity of DCFH-DA signal in the oocytes of PBS and DFO group. (n = 42–48). **J.** Relative fluorescence intensity of JC-1 red/green in the oocytes of PBS and DFO group. (n = 37–42). **K.** Relative fluorescence intensity of Annexin V signal in the oocytes of PBS and DFO group. (n = 38–40). Relative fluorescence intensity was compared to the PBS group. Twenty-four 12-month-old mice treated with PBS and twenty-four 12-month-old mice treated with DFO were used in this experiment. Data were presented as mean ± SEM of at least three times independent experiments. $^{*}P < 0.05$, $^{**}P < 0.01$.

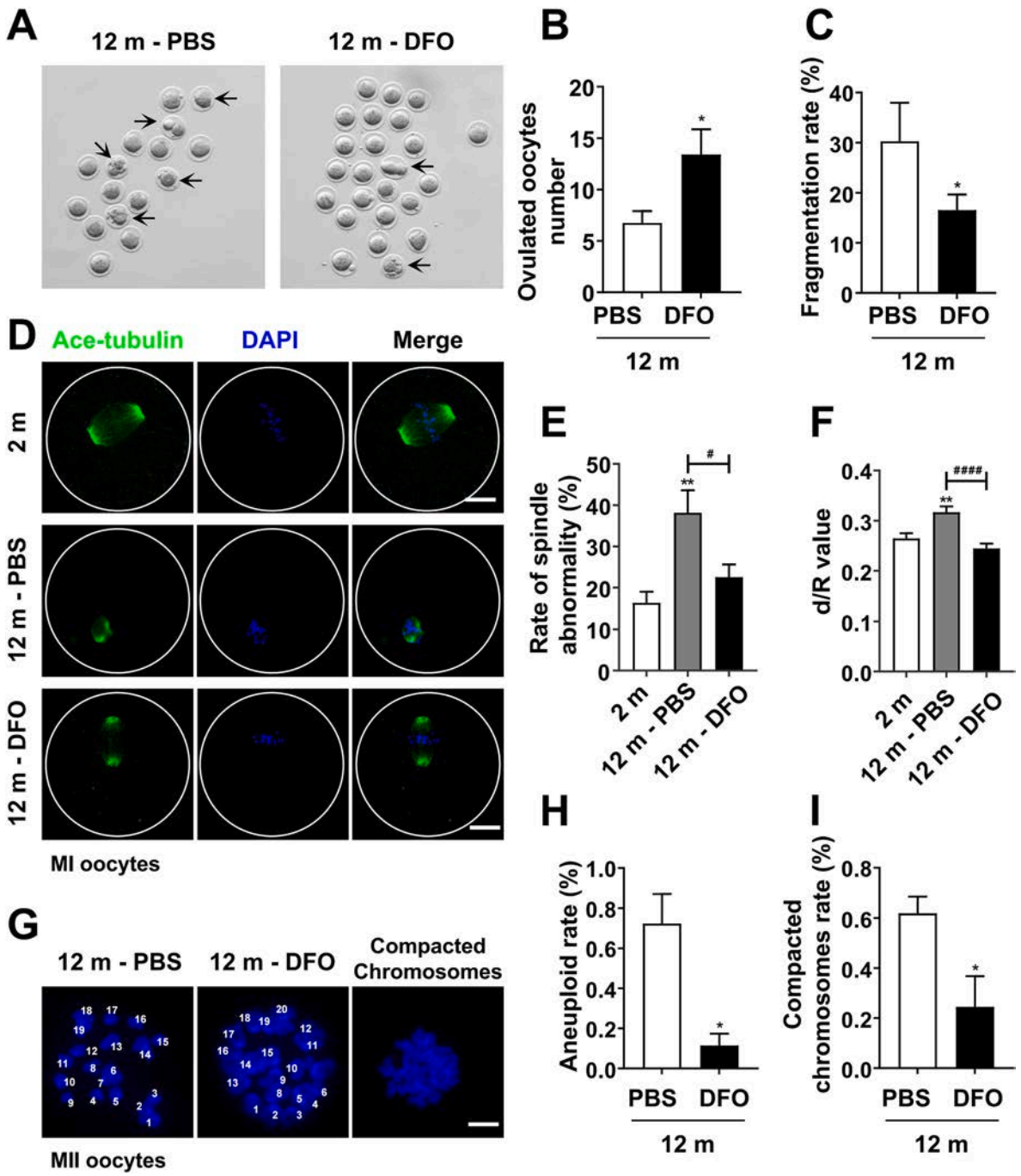

Fig. 13. DFO can improve the reproductive potential of aging mice. The 12 months mice were injected intraperitoneally with DFO for 14 days, while the control group was injected with PBS. **A.** Representative images of super-ovulated oocytes from mice in injected with PBS or DFO. The arrows point to fragmented oocytes. **B.** Statistical analysis of the number of super-ovulated oocytes in PBS and DFO group mice. (n = 6/group). **C.** Statistical analysis of fragmentation rate of oocytes in PBS and DFO group. (n = 6/group). **D.** Representative images of spindle in the oocytes of 2 m, 12 m - PBS and 12 m - DFO group. Scale bar = 10 μm. **E.** Statistical analysis of the rate of abnormal spindle in the oocytes from different groups. (n = 82–96). **F.** Statistical analysis of the d/R value of spindle in the oocytes from different groups. (n = 82–96). **G.** Representative images of chromosome spreading of MII oocytes in PBS and DFO group. Scale bar = 5 μm. **H.** Statistical analysis of aneuploid rate of MII oocytes in PBS and DFO group. (n = 8–23). **I.** Statistical analysis of the proportion of oocytes with compacted chromosomes in 12 m - PBS and 12 m - DFO groups. (n = 23–30). Data were presented as mean ± SEM of at least three times independent experiments. $^{*/\#}P < 0.05$, $^{**}P < 0.01$, $^{\#\#\#\#}P < 0.001$.

acid modifications in aging oocytes [65]. Though the levels of DNA damage, apoptosis and lipid peroxidation were increased in aging oocytes, the antioxidant enzyme GPX4 and Prx were not changed much except for an increase in SOD2. This suggests the overall antioxidant capacity is not collapsed, still able to resist ferroptosis in aging ovaries and oocytes. It can be considered that the main ROS type should be hydroxyl radical (•OH) from Fenton reaction, rather than superoxide radical ($O2^-$), as supported by the increase in lipid peroxidation index, including MDA, 4-HNE and 8-OHdG [66,67]. The anti-superoxide ability, as indicated by SOD2 and Prx, may be not the dominant force in resisting oxidative stress in aging ovaries.

All the ROS index and age-related degenerative changes were phenocopied in young oocytes treated with Fe^{2+} agent in vitro, and effectively ameliorated with combined application of DFO, an iron chelating drug. It is thus clear that iron is a net ROS producer in the intracellular environment [62]. In vivo administration of DFO could alleviate fibrotic

changes in aging ovaries, and slow down the decline in oocyte quantity and quality. This improvement may be based on the favorable turns in iron homeostasis and redox status, especially the recovery of mitophagy activity and mitochondrial potential. As reported, RAB7 works to balance mitophagy flux by suppressing Parkin activity [37], here we found DFO could increase RAB7 but decrease Parkin in mouse aging oocytes, thereby rectified the mitophagy activity, and recovered mitochondrial morphology and structure, as confirmed by improved JC-1 index. It may be reasonable to say that the age-related Fe^{2+} elevation plays a key role in oocyte aging and may be attributed to the dysregulated ferritinophagy and mitophagy. Besides oocytes, the granular cells also inevitably suffer Fe^{2+}-induced ROS and mitochondrial damages in aging ovaries, as well as in the pathological conditions of endometriosis and endometriosis, such injuries may be another facet of ovary degeneration [68].

In conclusion, the present study revealed disrupted iron metabolism and accumulation of iron in the ovaries and oocytes of aging mice, the application of iron chelating agent was showed to normalize intracellular Fe^{2+}, as well as modulate the activity of ferritinophagy and mitophagy activity, thereby this intervention effectively suppressed cellular oxidative stress and degenerative changes in aging oocytes. This study provides new perspectives and evidence for the understanding of fertility decline in elderly women and potential strategy for clinical intervention. It may possible to decrease the production of heme-derived iron by chemically inhibiting HO-1 or to reduce the iron content by using iron chelators, thereby alleviate iron overload and balance the redox status in the ovarian environment, so as to improve ovarian function in elder women.

CRediT authorship contribution statement

Ye Chen: Investigation, analysis and writing. **JiaqiZhang:** Methodology. **Xiangning Xu:** Methodology. **Bicheng Wang:** Data curation. **Ziqi Huang:** Software. **Shuo Lou:** Software. **Jingyi Kang:** Methodology. **Ningning Zhang:** Data curation. **Jing Weng:** Validation. **Yuanjing Liang:** Validation. **Wei Ma:** Conceptualization, analysis and writing.

Declaration of competing interest

The authors declare that they have no known competing financial interests or personal relationships that could have appeared to influence the work reported in this paper.

Data availability

No data was used for the research described in the article.

Acknowledgement

This work was supported by grants from National Natural Science Foundation of China (82071641 and 81671454) and the Natural Science Foundation of Beijing, China (7242003 and 7222002).

Appendix A. Supplementary data

Supplementary data to this article can be found online at https://doi.org/10.1016/j.redox.2024.103195.

References

[1] S. Wang, Y. Zheng, J. Li, Y. Yu, W. Zhang, M. Song, Z. Liu, Z. Min, H. Hu, Y. Jing, X. He, L. Sun, L. Ma, C.R. Esteban, P. Chan, J. Qiao, Q. Zhou, J.C. Izpisua Belmonte, J. Qu, F. Tang, G.H. Liu, Single-cell transcriptomic atlas of primate ovarian aging, Cell 180 (3) (2020) 585–600.
[2] Q. Li, X. Geng, W. Zheng, J. Tang, B. Xu, Q. Shi, Current understanding of ovarian aging, Sci. China Life Sci. 55 (8) (2012) 659–669.
[3] T.A. Ahmed, S.M. Ahmed, Z. El-Gammal, S. Shouman, A. Ahmed, R. Mansour, N. El-Badri, Oocyte aging: the role of cellular and environmental factors and impact on female fertility, Adv. Exp. Med. Biol. 1247 (2020) 109–123.
[4] F. Yan, Q. Zhao, Y. Li, Z. Zheng, X. Kong, C. Shu, Y. Liu, Y. Shi, The role of oxidative stress in ovarian aging: a review, J. Ovarian Res. 15 (1) (2022) 100.
[5] L. Wang, J. Tang, L. Wang, F. Tan, H. Song, J. Zhou, F. Li, Oxidative stress in oocyte aging and female reproduction, J. Cell. Physiol. 236 (12) (2021) 7966–7983.
[6] P.T. Goud, A.P. Goud, N. Joshi, E. Puscheck, M.P. Diamond, H.M. Abu-Soud, Dynamics of nitric oxide, altered follicular microenvironment, and oocyte quality in women with endometriosis, Fertil. Steril. 102 (1) (2014) 151–159 e155.
[7] H. Sasaki, T. Hamatani, S. Kamijo, M. Iwai, M. Kobanawa, S. Ogawa, K. Miyado, M. Tanaka, Impact of oxidative stress on age-associated decline in oocyte developmental competence, Front. Endocrinol. 10 (2019) 811.
[8] A.P. Goud, P.T. Goud, M.P. Diamond, B. Gonik, H.M. Abu-Soud, Reactive oxygen species and oocyte aging: role of superoxide, hydrogen peroxide, and hypochlorous acid, Free Radic. Biol. Med. 44 (7) (2008) 1295–1304.
[9] R.S. Zeidan, S.M. Han, C. Leeuwenburgh, R. Xiao, Iron homeostasis and organismal aging, Ageing Res. Rev. 72 (2021) 101510.
[10] M. Mazhar, A.U. Din, H. Ali, G. Yang, W. Ren, L. Wang, X. Fan, S. Yang, Implication of ferroptosis in aging, Cell Death Dis. 7 (1) (2021) 149.
[11] A. Agarwal, A. Aponte-Mellado, B.J. Premkumar, A. Shaman, S. Gupta, The effects of oxidative stress on female reproduction: a review, Reprod. Biol. Endocrinol. 10 (2012) 49.
[12] J. Li, F. Cao, H.L. Yin, Z.J. Huang, Z.T. Lin, N. Mao, B. Sun, G. Wang, Ferroptosis: past, present and future, Cell Death Dis. 11 (2) (2020) 88.
[13] K. Pantopoulos, S.K. Porwal, A. Tartakoff, L. Devireddy, Mechanisms of mammalian iron homeostasis, Biochemistry 51 (29) (2012) 5705–5724.
[14] G. Gao, J. Li, Y. Zhang, Y.Z. Chang, Cellular iron metabolism and regulation, Adv. Exp. Med. Biol. 1173 (2019) 21–32.
[15] K.T. Sawicki, A. De Jesus, H. Ardehali, Iron metabolism in cardiovascular disease: physiology, mechanisms, and therapeutic targets, Circ. Res. 132 (3) (2023) 379–396.
[16] S. Levi, M. Ripamonti, M. Dardi, A. Cozzi, P. Santambrogio, Mitochondrial ferritin: its role in physiological and pathological conditions, Cells 10 (8) (2021).
[17] G.J. Anderson, D.M. Frazer, Current understanding of iron homeostasis, Am. J. Clin. Nutr. 106 (Suppl 6) (2017) 1559S–1566S.
[18] M.D. Knutson, M.R. Vafa, D.J. Haile, M. Wessling-Resnick, Iron loading and erythrophagocytosis increase ferroportin 1 (FPN1) expression in J774 macrophages, Blood 102 (12) (2003) 4191–4197.
[19] D. Wang, Y. Hui, Y. Peng, L. Tang, J. Jin, R. He, Y. Li, S. Zhang, L. Li, Y. Zhou, J. Li, N. Ma, J. Li, S. Li, X. Gao, S. Luo, Overexpression of heme oxygenase 1 causes cognitive decline and affects pathways for tauopathy in mice, J Alzheimers Dis 43 (2) (2015) 519–534.
[20] F. Wang, J. Wang, Y. Shen, H. Li, W.D. Rausch, X. Huang, Iron dyshomeostasis and ferroptosis: a new alzheimer's disease hypothesis? Front. Aging Neurosci. 14 (2022) 830569.
[21] J. Velasquez, A.A. Wray, Deferoxamine. StatPearls. Treasure island (FL) ineligible companies, DisClosure: Anton Wray declares no relevant financial relationships with ineligible companies (2023).
[22] S. Rockfield, Y. Kee, M. Nanjundan, Chronic iron exposure and c-Myc/H-ras-mediated transformation in fallopian tube cells alter the expression of EVI1, amplified at 3q26.2 in ovarian cancer, Oncogenesis 8 (9) (2019) 46.
[23] L. Shen, J. Liu, A. Luo, S. Wang, The stromal microenvironment and ovarian aging: mechanisms and therapeutic opportunities, J. Ovarian Res. 16 (1) (2023) 237.
[24] A.M. Galvao, G. Ferreira-Dias, D.J. Skarzynski, Cytokines and angiogenesis in the corpus luteum, Mediat. Inflamm. 2013 (2013) 420186.
[25] T. Pedersen, H. Peters, Proposal for a classification of oocytes and follicles in the mouse ovary, J. Reprod. Fertil. 17 (3) (1968) 555–557.
[26] T. Hirayama, H. Tsuboi, M. Niwa, A. Miki, S. Kadota, Y. Ikeshita, K. Okuda, H. Nagasawa, A universal fluorogenic switch for Fe(ii) ion based on N-oxide chemistry permits the visualization of intracellular redox equilibrium shift towards labile iron in hypoxic tumor cells, Chem. Sci. 8 (7) (2017) 4858–4866.
[27] Y. Miao, Z. Cui, Q. Gao, R. Rui, B. Xiong, Nicotinamide mononucleotide supplementation reverses the declining quality of maternally aged oocytes, Cell Rep. 32 (5) (2020) 107987.
[28] X. Jiang, X. Xu, B. Wang, K. Song, J. Zhang, Y. Chen, Y. Tian, J. Weng, Y. Liang, W. Ma, Adverse effects of 2-Methoxyestradiol on mouse oocytes during reproductive aging, Chem. Biol. Interact. 369 (2023) 110277.
[29] K. Song, X. Jiang, X. Xu, Y. Chen, J. Zhang, Y. Tian, Q. Wang, J. Weng, Y. Liang, W. Ma, Ste20-like kinase activity promotes meiotic resumption and spindle microtubule stability in mouse oocytes, Cell Prolif. 56 (4) (2023) e13391.
[30] J. Fahrer, S. Wittmann, A.C. Wolf, T. Kostka, Heme oxygenase-1 and its role in colorectal cancer, Antioxidants 12 (11) (2023).
[31] S. Li, M. Wang, Y. Wang, Y. Guo, X. Tao, X. Wang, Y. Cao, S. Tian, Q. Li, p53-mediated ferroptosis is required for 1-methyl-4-phenylpyridinium-induced senescence of PC12 cells, Toxicol. Vitro 73 (2021) 105146.
[32] Q.Z. Tuo, P. Lei, K.A. Jackman, X.L. Li, H. Xiong, X.L. Li, Z.Y. Liuyang, L. Roisman, S.T. Zhang, S. Ayton, Q. Wang, P.J. Crouch, K. Ganio, X.C. Wang, L. Pei, P. A. Adlard, Y.M. Lu, R. Cappai, J.Z. Wang, R. Liu, A.I. Bush, Tau-mediated iron export prevents ferroptotic damage after ischemic stroke, Mol. Psychiatr. 22 (11) (2017) 1520–1530.
[33] X. Nie, Y. Dai, Y. Zheng, D. Bao, Q. Chen, Y. Yin, H. Fu, D. Hou, Establishment of a mouse model of premature ovarian failure using consecutive superovulation, Cell. Physiol. Biochem. 51 (5) (2018) 2341–2358.
[34] M. Kleih, K. Bopple, M. Dong, A. Gaissler, S. Heine, M.A. Olayioye, W.E. Aulitzky, F. Essmann, Direct impact of cisplatin on mitochondria induces ROS production that dictates cell fate of ovarian cancer cells, Cell Death Dis. 10 (11) (2019) 851.

[35] Y. Fang, X. Chen, Q. Tan, H. Zhou, J. Xu, Q. Gu, Inhibiting ferroptosis through disrupting the NCOA4-FTH1 interaction: a new mechanism of action, ACS Cent. Sci. 7 (6) (2021) 980–989.
[36] Z. Li, L. Jiang, S.H. Chew, T. Hirayama, Y. Sekido, S. Toyokuni, Carbonic anhydrase 9 confers resistance to ferroptosis/apoptosis in malignant mesothelioma under hypoxia, Redox Biol. 26 (2019) 101297.
[37] X. Jin, K. Wang, L. Wang, W. Liu, C. Zhang, Y. Qiu, W. Liu, H. Zhang, D. Zhang, Z. Yang, T. Wu, J. Li, RAB7 activity is required for the regulation of mitophagy in oocyte meiosis and oocyte quality control during ovarian aging, Autophagy 18 (3) (2022) 643–660.
[38] A. Caponnetto, R. Battaglia, C. Ferrara, M.E. Vento, P. Borzi, M. Paradiso, P. Scollo, M. Purrello, S. Longobardi, T. D'Hooghe, D. Valerio, C. Di Pietro, R.R. Italian Society of Embryology, Down-regulation of long non-coding RNAs in reproductive aging and analysis of the lncRNA-miRNA-mRNA networks in human cumulus cells, J. Assist. Reprod. Genet. 39 (4) (2022) 919–931.
[39] V. Camarena, T.C. Huff, G. Wang, Epigenomic regulation by labile iron, Free Radic. Biol. Med. 170 (2021) 44–49.
[40] A.S. Vogt, T. Arsiwala, M. Mohsen, M. Vogel, V. Manolova, M.F. Bachmann, On iron metabolism and its regulation, Int. J. Mol. Sci. 22 (9) (2021).
[41] F. Shaeib, J. Banerjee, D. Maitra, M.P. Diamond, H.M. Abu-Soud, Impact of hydrogen peroxide-driven Fenton reaction on mouse oocyte quality, Free Radic. Biol. Med. 58 (2013) 154–159.
[42] P.T. Goud, A.P. Goud, O.G. Camp, D. Bai, B. Gonik, M.P. Diamond, H.M. Abu-Soud, Chronological age enhances aging phenomena and protein nitration in oocyte, Front. Endocrinol. 14 (2023) 1251102.
[43] C. Fernandez-Mendivil, E. Luengo, P. Trigo-Alonso, N. Garcia-Magro, P. Negredo, M.G. Lopez, Protective role of microglial HO-1 blockade in aging: implication of iron metabolism, Redox Biol. 38 (2021) 101789.
[44] Y. Asano, Age-related accumulation of non-heme ferric and ferrous iron in mouse ovarian stroma visualized by sensitive non-heme iron histochemistry, J. Histochem. Cytochem. 60 (3) (2012) 229–242.
[45] S.C.W. Sze, L. Zhang, S. Zhang, K. Lin, T.B. Ng, M.L. Ng, K.F. Lee, J.K.W. Lam, Z. Zhang, K.K.L. Yung, Aberrant transferrin and ferritin upregulation elicits iron accumulation and oxidative inflammaging causing ferroptosis and undermines estradiol biosynthesis in aging rat ovaries by upregulating NF-Kappab-Activated inducible nitric oxide synthase: first demonstration of an intricate mechanism, Int. J. Mol. Sci. 23 (20) (2022).
[46] B. Galy, M. Conrad, M. Muckenthaler, Mechanisms controlling cellular and systemic iron homeostasis, Nat. Rev. Mol. Cell Biol. 25 (2) (2024) 133–155.
[47] D.H. Billhaq, S. Lee, The role of the guanosine nucleotide-binding protein in the corpus luteum, Animals (Basel) 11 (6) (2021).
[48] S. Li, M. Fujino, T. Takahara, X.K. Li, Protective role of heme oxygenase-1 in fatty liver ischemia-reperfusion injury, Med. Mol. Morphol. 52 (2) (2019) 61–72.
[49] S. Tonai, A. Kawabata, T. Nakanishi, J.Y. Lee, A. Okamoto, M. Shimada, Y. Yamashita, Iron deficiency induces female infertile in order to failure of follicular development in mice, J. Reprod. Dev. 66 (5) (2020) 475–483.
[50] G. Olivia, D.B. Camp, Pravin T. Goud, Michael P. Diamond, Husam M. Abu-Soud, A novel theory implicating hypochlorous acid as the primary generator of angiogenesis, infertility, and free iron in endometriosis, F&S Reviews 3 (2) (2022) 146–156.
[51] L. Gou, L. Zhao, W. Song, L. Wang, J. Liu, H. Zhang, Y. Huang, C.W. Lau, X. Yao, X. Y. Tian, W.T. Wong, J.Y. Luo, Y. Huang, Inhibition of miR-92a suppresses oxidative stress and improves endothelial function by upregulating heme oxygenase-1 in db/db mice, Antioxidants Redox Signal. 28 (5) (2018) 358–370.
[52] L.E. Otterbein, R. Foresti, R. Motterlini, Heme oxygenase-1 and carbon monoxide in the heart: the balancing act between danger signaling and pro-survival, Circ. Res. 118 (12) (2016) 1940–1959.
[53] S. Dutt, I. Hamza, T.B. Bartnikas, Molecular mechanisms of iron and heme metabolism, Annu. Rev. Nutr. 42 (2022) 311–335.
[54] J. Lim, U. Luderer, Oxidative damage increases and antioxidant gene expression decreases with aging in the mouse ovary, Biol. Reprod. 84 (4) (2011) 775–782.
[55] Y. Wang, H. Ding, Y. Zheng, X. Wei, X. Yang, H. Wei, Y. Tian, X. Sun, W. Wei, J. Ma, D. Tian, F. Zheng, Alleviated NCOA4-mediated ferritinophagy protected RA FLSs from ferroptosis in lipopolysaccharide-induced inflammation under hypoxia, Inflamm. Res. 73 (3) (2024) 363–379.
[56] M. Mezzanotte, G. Ammirata, M. Boido, S. Stanga, A. Roetto, Activation of the Hepcidin-Ferroportin1 pathway in the brain and astrocytic-neuronal crosstalk to counteract iron dyshomeostasis during aging, Sci. Rep. 12 (1) (2022) 11724.
[57] X. Qi, A. Song, M. Ma, P. Wang, X. Zhang, C. Lu, J. Zhang, S. Zheng, H. Jin, Curcumol inhibits ferritinophagy to restrain hepatocyte senescence through YAP/NCOA4 in non-alcoholic fatty liver disease, Cell Prolif. 54 (9) (2021) e13107.
[58] P.H. Lin, C.J. Li, L.T. Lin, W.P. Su, J.J. Sheu, Z.H. Wen, J.T. Cheng, K.H. Tsui, Unraveling the clinical relevance of ferroptosis-related genes in human ovarian aging, Reprod. Sci. 30 (12) (2023) 3529–3536.
[59] A. Anandhan, M. Dodson, A. Shakya, J. Chen, P. Liu, Y. Wei, H. Tan, Q. Wang, Z. Jiang, K. Yang, J.G. Garcia, S.K. Chambers, E. Chapman, A. Ooi, Y. Yang-Hartwich, B.R. Stockwell, D.D. Zhang, NRF2 controls iron homeostasis and ferroptosis through HERC2 and VAMP8, Sci. Adv. 9 (5) (2023) eade9585.
[60] M. Gryzik, A. Srivastava, G. Longhi, M. Bertuzzi, A. Gianoncelli, F. Carmona, M. Poli, P. Arosio, Expression and characterization of the ferritin binding domain of Nuclear Receptor Coactivator-4 (NCOA4), Biochim. Biophys. Acta Gen. Subj. 1861 (11 Pt A) (2017) 2710–2716.
[61] A. Esparza, Z.P. Gerdtzen, A. Olivera-Nappa, J.C. Salgado, M.T. Nunez, Iron-induced reactive oxygen species mediate transporter DMT1 endocytosis and iron uptake in intestinal epithelial cells, Am. J. Physiol. Cell Physiol. 309 (8) (2015) C558–C567.
[62] R. Ingrassia, B. Garavaglia, M. Memo, DMT1 expression and iron levels at the crossroads between aging and neurodegeneration, Front. Neurosci. 13 (2019) 575.
[63] R. Cinquetti, F.G. Imperiali, S. Bozzaro, D. Zanella, F. Vacca, C. Roseti, B. Peracino, M. Castagna, E. Bossi, Characterization of transport activity of SLC11 transporters in Xenopus laevis oocytes by fluorophore quenching, SLAS Discov 26 (6) (2021) 798–810.
[64] S. Buracco, B. Peracino, R. Cinquetti, E. Signoretto, A. Vollero, F. Imperiali, M. Castagna, E. Bossi, S. Bozzaro, Dictyostelium Nramp1, which is structurally and functionally similar to mammalian DMT1 transporter, mediates phagosomal iron efflux, J. Cell Sci. 128 (17) (2015) 3304–3316.
[65] S. Cheng, G. Altmeppen, C. So, L.M. Welp, S. Penir, T. Ruhwedel, K. Menelaou, K. Harasimov, A. Stutzer, M. Blayney, K. Elder, W. Mobius, H. Urlaub, M. Schuh, Mammalian oocytes store mRNAs in a mitochondria-associated membraneless compartment, Science 378 (6617) (2022) eabq4835.
[66] H. Zheng, L. Jiang, T. Tsuduki, M. Conrad, S. Toyokuni, Embryonal erythropoiesis and aging exploit ferroptosis, Redox Biol. 48 (2021) 102175.
[67] U. Urzua, C. Chacon, R. Espinoza, S. Martinez, N. Hernandez, Parity-dependent hemosiderin and lipofuscin accumulation in the reproductively aged mouse ovary, Anal. Cell Pathol. 2018 (2018) 1289103.
[68] Y. Wu, R. Yang, J. Lan, Y. Wu, J. Huang, Q. Fan, Y. You, H. Lin, X. Jiao, H. Chen, C. Cao, Q. Zhang, Iron overload modulates follicular microenvironment via ROS/HIF-1alpha/FSHR signaling, Free Radic. Biol. Med. 196 (2023) 37–52.